INTERNATIONAL JOURNAL FOR NUMERICAL METHODS IN FLUIDS, VOL. 23, 991–1020 (1996)

SENSITIVITY ANALYSIS AND OPTIMIZATION OF COUPLED THERMAL AND FLOW PROBLEMS WITH APPLICATIONS TO CONTRACTION DESIGN

ZI-XIAN WANG

Department of Theoretical and Applied Mechanics, University of Illinois, Urbana, IL 61801, U.S.A.

DANIEL A. TORTORELLI

Department of Mechanical and Industrial Engineering and Department of Theoretical and Applied Mechanics, University of Illinois, Urbana, IL 61801, U.S.A.

AND

JONATHAN A. DANTZIG

Department of Mechanical and Industrial Engineering, University of Illinois, Urbana, IL 61801, U.S.A.

SUMMARY

The finite element method and the Newton–Raphson solution algorithm are combined to solve the momentum, mass and energy conservation equations for coupled flow problems. Design sensitivities for a generalised response function with respect to design parameters which describe shape, material property and load data are evaluated via the direct differentiation method. The efficiently computed sensitivities are verified by comparison with computationally intensive, finite difference sensitivity approximations. The design sensitivities are then used in a numerical optimization algorithm to minimize the pressure drop in flow through contractions. Both laminar and turbulent flows are considered. In the turbulent flow problems the time-averaged momentum and mass conservation equations are solved using a mixing length turbulence model.

KEY WORDS: finite element analysis; design sensitivity analysis; optimization; contraction design

1. INTRODUCTION

The engineering design process is a vital component of industry, and recent efforts to improve competitiveness have brought design to the fore. Owing to the high cost of building prototypes, analysis is often used to evaluate and improve designs in the preliminary stages. In this paper we describe practical and efficient techniques for combining thermal and fluid flow analysis codes with numerical optimization to facilitate this preliminary design process. Because the individual process analyses are typically expensive to perform, we use optimization algorithms which require relatively few analyses. These algorithms use the design sensitivities of cost and constraint functions, and as such, much of this paper is devoted to the derivation of efficient means for computing these sensitivities. We then present some example problems for coupled thermal and fluid flow problems to illustrate the use of these techniques.

CCC 0271–2091/96/100991–30

Received 27 February 1995
Revised 13 October 1995

It is always possible to use zero-order optimization algorithms, i.e. algorithms which do not require sensitivities. Several authors have used this technique in aerodynamic design.[1–4] This approach is advantageous as it is easily implemented and does not require access to the analysis source code. However, we do not consider these algorithms to be a viable approach to design if the number of design parameters is large or the analyses are computationally intensive. Further, zero-order methods cannot guarantee that a design is optimal, as the Kuhn–Tucker optimality conditions cannot be verified.

Sensitivity analyses have been presented for numerous thermal problems. Haftka[5] and Meric[6–8] described sensitivity analysis for linear thermal systems, while Tortorelli and co-workers[9,10] and Dems[11,12] described an adjoint method for non-linear thermal systems. Direct differentiation approaches for transient, non-linear thermal systems are also presented in References 11–13. Relatively recently, sensitivity analyses have been presented for fluid flow systems. Many of these applications focus on aerodynamics, where the Euler equations are solved using finite difference or finite volume methods.[14–16] Others have considered the Navier–Stokes equations for low-Reynolds-number flows using both finite volume and finite element analysis methods.[17–20] We are not aware of any sensitivity analyses for higher-Reynolds-number turbulent flows.

The existence and interpretation of the sensitivities is an issue itself. Here we assume that the fluid/thermal system is differentiable with respect to the design. However, this is not always the case. In a plane flow, Fearn *et al.*[21] found that for an abrupt symmetric channel expansion and initially steady symmetric flow becomes asymmetrric and has multiple steady solutions as the Reynolds number increases. In such cases, sensitivity analysis cannot be performed, as the response is not differentiable with respect to the design. In addition, in turbulent and more general chaotic flows the response sensitivities are extreme. Indeed, the sensitivities with respect to the initial conditions can be used to identify chaotic responses. The use of these extreme sensitivities in a Taylor series expansion or an optimization algorithm would appear to be fruitless. However, if temporal or spatial statistical response measures are used (which are not extremely sensitive to the initial conditions), then we expect that their sensitivities will be meaningful.

In the following sections we present a systematic approach for computing explicit design sensitivity for transient laminar flows, coupled with the solution of the energy equation. Sensitivities for a general functional are evaluted with respect to shape, material response and load data parameters. These methods are then extended to consider turbulent flows, using a mixing length model for the eddy viscosity in the time-averaged form of the Navier–Stokes equations.

The mixing length model has been largely supplanted by the k–ε model of Launder and Spalding[22,23] in many applications. However, shape sensitivity analysis for this model proved to be extremely difficult owing to its use of special wall elements and specialized shape functions to represent turbulent boundary layers. The mixing length model is computationally simpler than the k–ε models and is adequate for simple geometries and non-recirculating flows.[24]

After deriving expressions for the efficient computation of design sensitivities for these flows, we consider the design of an axisymmetric contraction. The pipe profile in the transition region is designed to minimize the pressure loss through the contraction. As one might expect, laminar and turbulent flows require considerably different profiles to achieve this goal.

2. BASIC FORMULATIONS

This section outlines the basic equations used to derive shape sensitivities, the means to solve non-linear problems and a general approach to evaluate design sensitivities for both steady state and transient coupled flow systems.

2.1. Domain parametrization overview

The domain parametrization method is incorporated to evaluate shape sensitivities. In this method (see Reference 25 for further details) all fields are transformed from the current configuration b with boundary ∂b and outward normal $\mathbf{n}$ to a fixed reference configuration B with boundary ∂B and outward normal $\mathbf{N}$. The transformation is accomplished through the map $\boldsymbol{\chi}$:

$$\mathbf{x} = \boldsymbol{\chi}(\mathbf{X}, \boldsymbol{\Phi}) = \sum_{I=1}^{N_e} \boldsymbol{\Psi}^I(\mathbf{X}) x^I(\boldsymbol{\Phi}), \tag{1}$$

where $\mathbf{x}$ is the position of a material point in the current configuration (here the spatial configuration), $\mathbf{X}$ is the position of the matrial point in the reference configuration and $\boldsymbol{\Phi}$ is the design parameter vector. In the finite element method the map $\boldsymbol{\chi}$ is expressed piecewise over the domain through ψ^I, the element shape function associated with the I th node, x^I, the I th element node co-ordinate vector, and N_e, the number of nodes which comprise the element. Note that x^I is a function of the design parameters. The Jacobian is defined in the usual fashion as

$$\mathbf{J}(\mathbf{X}, \boldsymbol{\Phi}) = \nabla \boldsymbol{\chi}_{\mathbf{X}}(\mathbf{X}, \boldsymbol{\Phi}). \tag{2}$$

The Jacobian determinant $J(\mathbf{X}, \boldsymbol{\Phi}) = \det(\mathbf{J}(\mathbf{X}, \boldsymbol{\Phi}))$ is used to relate differential volumes between the two configurations in the usual manner, whereas differential areas da_X on ∂B and da_x on $\partial b = \boldsymbol{\chi}(\partial B, \boldsymbol{\Phi})$ are related through the surface area metric K as

$$K(\mathbf{X}, \boldsymbol{\Phi}) = da_x / da_X = J(\mathbf{X}, \boldsymbol{\Phi}) \| \mathbf{J}^{-T}(\mathbf{X}, \boldsymbol{\Phi}) \mathbf{N}(\mathbf{X}) \|. \tag{3}$$

All functions T defined on the current configuration b are transformed to referential functions $\hat{T}$ defined on the reference configuration B through the composition

$$\hat{T}(\mathbf{X}, \boldsymbol{\Phi}) = T(\boldsymbol{\chi}(\mathbf{X}, \boldsymbol{\Phi}), \boldsymbol{\Phi}). \tag{4}$$

Note that while functions $\hat{T}$ and T differ (indeed, they are defined on different domains), their values agree at the corresponding pairs $(\mathbf{X}, \boldsymbol{\Phi})$ and $(\boldsymbol{\chi}(\mathbf{X}, \boldsymbol{\Phi}), \boldsymbol{\Phi})$.

2.2. Newton–Raphson method

The Newton–Raphson method is an effective means to solve non-linear problems (see Reference 26 for more details). Additionally, the tangent operator used in the Newton–Raphson iteration is also used in the sensitivity analysis.

We express the non-linear problem (here the coupled flow problem) in residual form as

$$\mathbf{R}(\mathbf{U}(\boldsymbol{\Phi}), \boldsymbol{\Phi}) = \mathbf{0}, \tag{5}$$

where $\mathbf{R}$ is the discretized residual and $\mathbf{U}$ is the discretized system response. In the Newton–Raphson analysis, equation (5) is solved iteratively for $\mathbf{U}$ for a fixed design $\boldsymbol{\Phi}$. The current iterate $\mathbf{U}^I$ is updated to $\mathbf{U}^{I+1}(\boldsymbol{\Phi}) = \mathbf{U}^I(\boldsymbol{\Phi}) + \mathrm{d}\mathbf{U}$, where the incremental response $\mathrm{d}\mathbf{U}$ is the solution to the linearized problem

$$\frac{\partial \mathbf{R}}{\partial \mathbf{U}}(\mathbf{U}^I(\boldsymbol{\Phi}), \boldsymbol{\Phi}))\mathrm{d}\mathbf{U} = -\mathbf{R}(\mathbf{U}^I(\boldsymbol{\Phi}), \boldsymbol{\Phi}), \tag{6}$$

in which $\partial \mathbf{R}/\partial \mathbf{U}$ is the tangent operator. This process is repeated until convergence is attained and is generally regarded as highly effective since it exhibits quadratic terminal convergence.[27]

2.3. *Direct differentiation sensitivity analysis*

Three techniques have been used in the literature to evaluate sensitivities: the finite difference, direct differentiation and adjoint methods. Although the finite difference method is the easiest to implement, it is computationally inefficient and may suffer from round-off or truncation errors.[28] On the other hand, the direct differentiation and adjoint methods are both computationally efficient and accurate. The choice between the direct and adjoint methods generally depends on the ratio of the number of design parameters to the number of response functions. If the number of response functions exceeds the number of design parameters, the direct differentiation method is preferred; otherwise the adjoint method is preferred.[28] In addition, transient systems may favour the direct differentiation method owing to the backward time mappings which are required in the adjoint method.[13] Here the direct differentiation method is selected for the sensitivity analyses so that transients may be easily incorporated.

In the following (see Reference 26 for more details) we consider a generalized response function written as

$$G(\mathbf{U}(\mathbf{\Phi}), \mathbf{\Phi}), \tag{7}$$

where $\mathbf{\Phi}$ is the design parameter vector. For the coupled flow problem the response $\mathbf{U}$ consists of the velocity, temperature, pressure, stress, velocity gradient, internal energy, heat flux and temperature gradient fields, while the design parameters in $\mathbf{\Phi}$ may be used to describe the shape, material response and load data.

The design sensitivity is computed from

$$\frac{\mathrm{D}G}{\mathrm{D}\mathbf{\Phi}} = \frac{\partial G}{\partial \mathbf{U}} \frac{\mathrm{D}\mathbf{U}}{\mathrm{D}\mathbf{\Phi}} + \frac{\partial G}{\partial \mathbf{\Phi}}. \tag{8}$$

In the above, $\partial G/\partial \mathbf{U}$ and $\partial G/\partial \mathbf{\Phi}$ are explicitly known quantities since G is defined by the engineer, whereas $\mathrm{D}\mathbf{U}/D\mathbf{\Phi}$ is implicit because $\mathbf{U}$ is implicitly defined on the design through the system equation (see equation (5)).

In the direct differentiation sensitivity analysis the response derivative $\mathrm{D}\mathbf{U}/D\mathbf{\Phi}$ is evaluated, whereupon the sensitivity may be evaluated from equation (8). Differentiation of equation (5) with respect to each of the N design parameters and some rearrangement yields

$$\frac{\partial \mathbf{R}}{\partial \mathbf{U}} \frac{\mathrm{D}\mathbf{U}}{\mathrm{D}\Phi_i} = -\frac{\partial \mathbf{R}}{\partial \Phi_i}. \tag{9}$$

The response sensitivities $\mathrm{D}\mathbf{U}/\mathrm{D}\Phi_i$ are evaluated by solving the above pseudoproblems which are linear in $\mathrm{D}\mathbf{U}/\mathrm{D}\Phi_i$. Here $\partial \mathbf{R}/\partial \mathbf{U}$ is the same tangent operator which is used in the Newton–Raphson method (see equation (6)) and the $-\partial \mathbf{R}/\partial \Phi_i$ define the so-called pseudoloads. Once all the response sensitivities $\mathrm{D}\mathbf{U}/\mathrm{D}\Phi_i$ are determined, the sensitivities for any number of response functions may be evaluated from equation (8).

As previously mentioned, the tangent operator required for the Newton–Raphson method is also required to compute the sensitivities (see equations (6) and (9)). Therefore in the finite element method the decomposed tangent stiffness matrix resulting from the iterative solution of $\mathbf{U}$ may again be used to solve equation (9) for each of the $\mathrm{D}\mathbf{U}/\mathrm{D}\Phi_i$. Hence, whereas the iterative solution of the primal anlaysis for $\mathbf{U}$ requires many matrix assemblies, decompositions and back substitutions, the evaluations of the $\mathrm{D}\mathbf{U}/\mathrm{D}\Phi_i$ require only the formation of N pseudoload vectors $(-\partial \mathbf{R}/\partial \Phi_i)$ followed by N back

substitutions.* Thus the direct differentiation method is cost-efficient. Furthermore, since no approximation to the derivative is used, the direct differentiation method is not degraded by the truncation or round-off errors that afflict the finite difference method.

2.4. Discrete transient sensitivity anlaysis

For transient problems the system is described by the response $\mathbf{U}$ (a function of time) and its time derivatives. To solve a transient problem numerically, we discretize the time domain into a finite number of intervals and obtain the time derivatives by finite difference approximations.

Fully implicit (backward Euler) time integration is incorporated here owing to its stability.[29,30] The response time derivative is approximated by the backward difference†

$$ {}^{n}\dot{\mathbf{U}} \approx \frac{{}^{n}\mathbf{U} - {}^{n-1}\mathbf{U}}{{}^{n}t - {}^{n-1}t}, \tag{10} $$

where for a typical time step n the quantities ${}^{n-1}\mathbf{U}$ and ${}^{n}\mathbf{U}$ refer to the responses at the beginning and end of the time step respectively, i.e. at times ${}^{n-1}t$ and ${}^{n}t$. Consequently, the discretized residual ${}^{n}\mathbf{R}$ is a function of the unknown response ${}^{n}\mathbf{U}$ (to be evaluated during the time ${}^{n}t$ analysis), the known response ${}^{n-1}\mathbf{U}$ (since it is computed at the previous time step ${}^{n-1}t$ analysis) and the known design Φ (since it is fixed during the analysis), i.e.

$$ {}^{n}\mathbf{R}({}^{n}\mathbf{U}(\Phi), {}^{n-1}\mathbf{U}(\Phi), \Phi) = \mathbf{0}. \tag{11} $$

To solve equation (11) for ${}^{n}\mathbf{U}$, we again use the Newton–Raphson method. The iterations are repeated for the time ${}^{n}t$ analysis until the solution converges, at which point the time is advanced.

For the discretized transient problem (see Reference 26 for more details) the response function is written in terms of the solution at the discrete times ${}^{0}t, {}^{1}t, {}^{2}t, \ldots, {}^{M}t$ as

$$ G({}^{M}\mathbf{U}(\Phi), {}^{M-1}\mathbf{U}(\Phi), \ldots, {}^{1}\mathbf{U}(\Phi), {}^{0}\mathbf{U}(\Phi), \Phi), \tag{12} $$

where ${}^{M}t = t_f$ is the terminal analysis time and ${}^{0}t = 0$ is the initial analysis time. The response at intermediate times may be incorporated by interpolation in the time domain. The sensitivity of G is obtained by differentiating equation (12):

$$ \frac{\mathrm{D}G}{\mathrm{D}\Phi_i} = \sum_{n=0}^{M} \frac{\partial G}{\partial({}^{n}\mathbf{U})} \frac{\mathrm{D}({}^{n}\mathbf{U})}{\mathrm{D}\Phi_i} + \frac{\partial G}{\partial \Phi_i}, \tag{13} $$

where the response sensitivities $\mathrm{D}({}^{n}\mathbf{U})/\mathrm{D}\Phi_i$ are all implicit quantities which must be resolved.

To evaluate the response sensitivity $\mathrm{D}({}^{n}\mathbf{U})/\mathrm{D}\Phi_i$, we may apply the direct differentiation method. Equation (11) is differentiated with respect to Φ_i, which after some rearranging yields

$$ \frac{\partial({}^{n}\mathbf{R})}{\partial({}^{n}\mathbf{U})} \frac{\mathrm{D}({}^{n}\mathbf{U})}{\mathrm{D}\Phi_i} = -\frac{\partial({}^{n}\mathbf{R})}{\partial({}^{n-1}\mathbf{U})} \frac{\mathrm{D}({}^{n-1}\mathbf{U})}{\mathrm{D}\Phi_i} - \frac{\partial({}^{n}\mathbf{R})}{\partial \Phi_i}. \tag{14} $$

---

* In the Newton–Raphson iteration the tangent operator is evaluated at the previous solution iterate $\mathbf{U}^{l-1}$. However, in the pseudoproblem the derivative $\mathrm{D}\mathbf{U}/\mathrm{D}\Phi_i$ is evaluated at the converged solution $\mathbf{U}^{l}$. Therefore, if $\mathbf{U}^{l-1}$ and $\mathbf{U}^{l}$ are significantly different, then $\partial\mathbf{R}/\partial\mathbf{U}$ should be re-evaluated and decomposed once before proceeding with the N pseudoanalyses.

† The notation ${}^{n}f = f({}^{n}t)$ is used henceforth.

The response sensitivity $D({}^n\mathbf{U})/D\Phi_i$ is evaluated by solving the above pseudoproblems, where again $\partial({}^n\mathbf{R})/\partial({}^n\mathbf{U})$ is the tangent operator which is formed during the primal anlaysis at time ${}^nt$ and

$$-\left(\frac{\partial({}^n\mathbf{R})}{\partial({}^{n-1}\mathbf{U})}\frac{D({}^{n-1}\mathbf{U})}{D\Phi_i}+\frac{\partial({}^n\mathbf{R})}{\partial\Phi_i}\right)$$

is the pseudoload. It is presumed in equation (14) that $D({}^{n-1}\mathbf{U})/D\Phi_i$ is a known quantity. This poses no problem, for at the initial analysis, i.e. $n = 1$, $D({}^0\mathbf{U})/D\Phi_i$ is known since it is the design derivative of the initial condition. Then $D({}^1(\mathbf{U})/D\Phi_i$ is obtained from equation (14) for $n = 1$. This procedure is repeated at each time step until $D({}^{n-1}\mathbf{U})/D\Phi_i$ is determined. Consequently, the evaluations of the primal response ${}^n\mathbf{U}$ and response sensitivities $D({}^n\mathbf{U})/D\Phi_i$ are performed simultaneously.

The finite element procedure to compute the direct differentiation sensitivities proceeds as follows. At each time step ${}^nt$ the resonse ${}^n\mathbf{U}$ is first evaluated via a Newton–Raphson iteration. Then the N pseudoload vectors of equation (14) are formed and back substituted into the existing decomposed tangent stiffness matrix to evaluate the response sensitivities $D({}^n\mathbf{U})/D\Phi_i$. Finally, the sensitivity is computed from equation (13). The statements regarding the accuracy and efficiency of the steady state sensitivity also apply here.

3. COUPLED FLOW PROBLEMS

3.1. Governing equations

The mass, momentum and energy conservation equations are expressed in terms of the velocity, temperature and pressure fields in what is sometimes called the 'mixed method'. The corresponding equations which use the penalty method to eliminate the pressure field are provided in Appendix I. Using a Eulerian kinematic description and a constant density fluid, the coupled flow problem is[31]

$$\begin{aligned}\rho\left(\frac{\partial\mathbf{u}}{\partial t}+(\nabla_{\mathbf{x}}\mathbf{u})\mathbf{u}\right)&=\mathrm{div}_{\mathbf{x}}\boldsymbol{\tau}+\rho\mathbf{b}\quad\text{in } b\times I\times\mathscr{R}^N,\\ \rho\left(\frac{\partial e(T)}{\partial t}+\mathbf{u}\cdot\nabla_{\mathbf{x}}e(T)\right)&=-\mathrm{div}_{\mathbf{x}}\mathbf{q}+\boldsymbol{\tau}\cdot\nabla_{\mathbf{x}}\mathbf{u}+\rho Q(T)\quad\text{in } b\times I\times\mathscr{R}^N,\\ \mathrm{div}_{\mathbf{x}}(\mathbf{u})&=0\quad\text{in } b\times I\times\mathscr{R}^N,\end{aligned}\tag{15}$$

where all field quantities are functions of $(\mathbf{x}, t, \boldsymbol{\Phi}) \in b \times I \times \mathscr{R}^N$, i.e. the spatial location $\mathbf{x} \in b$, the time $t \in I = [0, t_f]$ and the design $\boldsymbol{\Phi} \in \mathscr{R}^N$. The internal energy per unit mass, e, and heat source Q may be temperature-dependent. In the momentum equation, $\mathbf{b}$ is the body force per unit mass, which may represent gravity, Lorenz forces or a D'Alembert body force. Also in the above equations, $\mathbf{u}$, $\boldsymbol{\tau}$, ρ and $\mathbf{q}$ are the velocity vector, Cauchy stress tensor, density and heat flux vector fields respectively.

In addition, we first consider the following constitutive laws to be enforced: a Newtonian fluid relation and a non-linear Fourier conductivity relation

$$\begin{aligned}\boldsymbol{\tau}(p,\mathbf{D},T)&=-p\mathbf{I}+2\mu(T)\mathbf{D}\quad\text{in } b\times I\times\mathscr{R}^N,\\ \mathbf{q}(T,\mathbf{g})&=-\mathbf{k}(T)\mathbf{g}(T)\quad\text{in } b\times I\times\mathscr{R}^N,\end{aligned}\tag{16}$$

where μ is the temperature-dependent viscosity, $\mathbf{k}$ is the temperature-dependent thermal conductivity tensor, p is the pressure, $\mathbf{D} = \frac{1}{2}[\nabla_{\mathbf{x}}\mathbf{u} + (\nabla_{\mathbf{x}}\mathbf{u})^T]$ is the rate-of-deformation tensor and $\mathbf{g} = \nabla_{\mathbf{x}}T$ is the temperature gradient vector.

Finally, the boundary conditions

$$\begin{aligned} \mathbf{u} &= \mathbf{u}^{\mathrm{p}} \quad \text{on } a_u \times I \times \mathscr{R}^N, \\ \mathbf{t} &= \mathbf{t}^{\mathrm{p}} \quad \text{on } a_t \times I \times \mathscr{R}^N, \\ T &= T^{\mathrm{p}} \quad \text{on } a_T \times I \times \mathscr{R}^N, \\ q^{\mathrm{s}} &= q^{\mathrm{p}}(T) \quad \text{on } a_q \times I \times \mathscr{R}^N \end{aligned} \tag{17}$$

and the initial conditions

$$\begin{aligned} \mathbf{u}|_{t=0} &= \mathbf{u}^0 \quad \text{in } b \times \mathscr{R}^N, \\ T|_{t=0} &= T^0 \quad \text{in } b \times \mathscr{R}^N \end{aligned} \tag{18}$$

are enforced. In the above, $\mathbf{t} \equiv \boldsymbol{\tau}\mathbf{n}$ is the stress vector and $q^{\mathrm{s}} \equiv \mathbf{q} \cdot \mathbf{n}$ is the outward surface heat flux. In the natural boundary condition on a_q, q^{p} is expressed in a general form so that it can be used to model prescribed flux, convective and radiation boundary conditions.

The primary response consists of the spatial velocity vector $\mathbf{u}$, temperature T and pressure p. The other (derived) spatial response fields consist of the Cauchy stress $\boldsymbol{\tau}$, rate-of-deformation tensor $\mathbf{D}$, stress vector $\mathbf{t}$, heat flux vector $\mathbf{q}$, temperature gradient $\mathbf{g}$ and surface heat flux q^{s}. Explicitly defined field quantities (which can be parametrized by the design parameters $\boldsymbol{\Phi}$) consist of the prescribed velocity vector $\mathbf{u}^{\mathrm{p}}$, prescribed surface traction vector $\mathbf{t}^{\mathrm{p}}$, prescribed temperature T^{p}, initial velocity vector $\mathbf{u}^0$ and initial temperature T^0. Finally, the following fields exhibit explicit dependence on the design and possibly implicit dependence on the response owing to temperature dependence: the body force vector $\mathbf{b}$, viscosity μ, heat source Q, internal energy per unit mass, e, thermal conductivity tensor $\mathbf{k}$ and heat flux q^{p}.

Following the usual isoparametric finite element formulation and the implicit time integration scheme described above, we define the variational statement corresponding to the coupled flow problem on the reference configuration B at time ${}^n t$ as

$$\begin{aligned} {}^nR({}^n\hat{\mathbf{u}}, {}^{n-1}\hat{\mathbf{u}}, {}^n\hat{T}, {}^{n-1}\hat{T}, {}^n\hat{p}, {}^{n-1}\hat{p}) = & \int_B \bar{\mathbf{u}} \cdot \hat{\rho}\left(\frac{{}^n\hat{\mathbf{u}} - {}^{n-1}\hat{\mathbf{u}}}{\Delta t} + \nabla_{\mathbf{X}}{}^n\hat{\mathbf{u}}\mathbf{J}^{-1}{}^n\hat{\mathbf{u}} - {}^n\hat{\mathbf{b}}\right) J \mathrm{d}v_{\mathbf{X}} \\ & + \int_B [-{}^n\hat{p}\mathbf{I} \cdot \hat{\mathbf{D}}(\bar{\mathbf{u}}, \mathbf{J}) + \hat{\mathbf{D}}(\bar{\mathbf{u}}, \mathbf{J}) \cdot 2\hat{\mu}\hat{\mathbf{D}}({}^n\hat{\mathbf{u}}, \mathbf{J})] J \mathrm{d}v_{\mathbf{X}} \\ & + \int_B \bar{T}\hat{\rho}\left(\frac{{}^n\hat{e} - {}^{n-1}\hat{e}}{\Delta t} + {}^n\hat{\mathbf{u}} \cdot \mathbf{J}^{-\mathrm{T}}\nabla_{\mathbf{X}}{}^n\hat{\mathbf{e}} - {}^n\hat{Q}\right) J \mathrm{d}_{\mathbf{X}} \\ & - \int_B \bar{T}\{\hat{\mathbf{D}}({}^n\hat{\mathbf{u}}, \mathbf{J}) \cdot [-{}^n\hat{p}\mathbf{I} + 2\hat{\mu}\hat{\mathbf{D}}({}^n\hat{\mathbf{u}}, \mathbf{J})]\} J \mathrm{d}v_{\mathbf{X}} \\ & + \int_B \hat{\mathbf{g}}(\bar{T}, \mathbf{J}) \cdot \hat{\mathbf{k}}\hat{\mathbf{g}}({}^n\hat{T}, \mathbf{J}) J \mathrm{d}v_{\mathbf{X}} + \int_{A_q} \bar{T}{}^n\hat{q}^{\mathrm{p}} K \mathrm{d}a_{\mathbf{X}} \\ & + \int_B \bar{p}\mathbf{I} \cdot \hat{\mathbf{D}}({}^n\hat{\mathbf{u}}, \mathbf{J}) J \mathrm{d}v_{\mathbf{X}} - \int_{A_t} \bar{\mathbf{u}} \cdot {}^n\hat{\mathbf{t}}^{\mathrm{p}} K \mathrm{d}a_{\mathbf{X}} \\ = & \ 0, \end{aligned} \tag{19}$$

where $\hat{(\ )}$ denotes a referential field quantity (see equation (4)). The referential kinematically admissible weighting functions $\bar{\mathbf{u}}$ and $\bar{T}$ have spatial derivatives which are square integrable and satisfy $\bar{\mathbf{u}} = 0$ and $\bar{T} = 0$ on the surface A_u and A_T respectively. The field $\bar{p}$ is kinematically admissible if it is

square integrable.[32] Likewise, $\hat{\mathbf{u}}$ and $\hat{T}$ are kinematically admissssible if their spatial derivatives are square integrable and they satisfy the essential boundary conditions on the surfaces A_u and A_T respectively, and $\hat{p}$ is kinematically admissible if it is square integrable.

In equation (19) the referential rate-of-deformation tensor $\hat{\mathbf{D}}$ and referential temperature gradient vector $\hat{\mathbf{g}}$ are defined via

$$\begin{aligned} \hat{\mathbf{D}}(\hat{\mathbf{u}}, \mathbf{J}) &= \tfrac{1}{2}[\nabla_{\mathbf{X}}\hat{\mathbf{u}}\mathbf{J}^{-1} + \mathbf{J}^{-T}(\nabla_{\mathbf{X}}\hat{\mathbf{u}})^{\mathrm{T}}], \\ \hat{\mathbf{g}}(\hat{T}, \mathbf{J}) &= \mathbf{J}^{-T}\nabla_{\mathbf{x}}\hat{T}, \end{aligned} \tag{20}$$

and similarly for $\hat{\mathbf{D}}(\hat{\mathbf{u}}, \mathbf{J})$ and $\hat{\mathbf{g}}(\bar{T}, \mathbf{J})$.

To show that equation (19) is of the form of equation (11), we define

$${}^{n}\mathbf{U}(\mathbf{\Phi}) = ({}^{n}\hat{\mathbf{u}}(\mathbf{\Phi}), {}^{n}\hat{T}(\mathbf{\Phi}), {}^{n}\hat{p}(\mathbf{\Phi})). \tag{21}$$

The tangent operator may then be evaluated in partitioned form from

$$\frac{\partial({}^{n}R)}{\partial({}^{n}\mathbf{U})}\mathrm{d}\mathbf{U} = \left(\frac{\partial({}^{n}R)}{\partial({}^{n}\hat{\mathbf{u}})}\frac{\partial({}^{n}R)}{\partial({}^{n}\hat{T})}\frac{\partial({}^{n}R)}{\partial({}^{n}\hat{p})}\right)\begin{pmatrix}\mathrm{d}\hat{\mathbf{u}}\\ \mathrm{d}\hat{T}\\ \mathrm{d}\hat{p}\end{pmatrix},$$

where the detailed derivative expressions appear in Appendix II.

3.2. *Sensitivity analysis for the mixed method*

For the coupled flow problem the generalized response function is expressed (after discretization in time and transformation to the reference configuration) as

$$\begin{aligned} G(\mathbf{\Phi}) = &\int_B \hat{F}({}^{M}\hat{\mathbf{u}}(\mathbf{\Phi}), {}^{M}\hat{\boldsymbol{\tau}}(\mathbf{\Phi}), {}^{M}\hat{\mathbf{D}}(\mathbf{\Phi}), {}^{M}\hat{p}(\mathbf{\Phi}), {}^{M}\hat{T}(\mathbf{\Phi}), {}^{M}\hat{e}(\mathbf{\Phi}), {}^{M}\hat{\mathbf{q}}(\mathbf{\Phi}), {}^{M}\hat{\mathbf{g}}(\mathbf{\Phi}), \mathbf{\Phi})J(\mathbf{\Phi})\mathrm{d}v_{\mathbf{X}} \\ &+ \int_A \hat{h}({}^{M}\hat{\mathbf{u}}(\mathbf{\Phi}), {}^{M}\hat{\mathbf{t}}(\mathbf{\Phi}), {}^{M}\hat{T}(\mathbf{\Phi}), {}^{M}\hat{\mathbf{q}}^{s}(\mathbf{\Phi}), \mathbf{\Phi})K(\mathbf{\Phi})\mathrm{d}a_{\mathbf{X}}, \end{aligned} \tag{22}$$

where for conciseness the spatial dependence has been omitted and only the response at time ${}^{M}t = t_{\mathrm{f}}$ is incorporated in G. However, this latter simplification does not present a limitation to the method, as the response at any or all time steps may be readily incorporated. Furthermore, G may include time integration to evaluate e.g. average values over time a interval.

To simplify the ensuing sensitivity analysis, we partition the design vector as the set product of shape, $\mathbf{\Phi}_{\mathrm{s}}$, material property, $\mathbf{\Phi}_{\mathrm{m}}$, and load data, $\mathbf{\Phi}_{\mathrm{ld}}$, parameter vectors, i.e.

$$\mathbf{\Phi} = (\mathbf{\Phi}_{\mathrm{s}}, \mathbf{\Phi}_{\mathrm{m}}, \mathbf{\Phi}_{\mathrm{ld}})^{\mathrm{T}}. \tag{23}$$

Expressions for the derivatives $\partial G/\partial\mathbf{\Phi}$ and $\partial G/\partial({}^{M}\mathbf{U})$ which are required to evaluate the sensitivities (see equation (13)) are provided in Appendix II.

To obtain the response design derivatives

$$\frac{\partial({}^{n}\mathbf{U})}{\partial\mathbf{\Phi}} = \left(\frac{\partial({}^{n}\mathbf{U})}{\partial\mathbf{\Phi}_{\mathrm{s}}}, \frac{\partial({}^{n}\mathbf{U})}{\partial\mathbf{\Phi}_{\mathrm{m}}}, \frac{\partial({}^{n}\mathbf{U})}{\partial\mathbf{\Phi}_{\mathrm{ld}}}\right),$$

we combine equations (14), (21) and (23) to give

$$\left[\frac{\partial({}^n R)}{\partial({}^n\hat{\mathbf{u}})} \quad \frac{\partial({}^n R)}{\partial({}^{n-1}\hat{T})} \quad \frac{\partial({}^n R)}{\partial({}^n\hat{p})}\right]\begin{pmatrix} \frac{\partial({}^n\hat{\mathbf{u}})}{\partial\boldsymbol{\Phi}_s} & \frac{\partial({}^n\hat{\mathbf{u}})}{\partial\boldsymbol{\Phi}_m} & \frac{\partial({}^n\hat{\mathbf{u}})}{\partial\boldsymbol{\Phi}_{ld}} \\ \frac{\partial({}^n\hat{T})}{\partial\boldsymbol{\Phi}_s} & \frac{\partial({}^n\hat{T})}{\partial\boldsymbol{\Phi}_m} & \frac{\partial({}^n\hat{T})}{\partial\boldsymbol{\Phi}_{ld}} \\ \frac{\partial({}^n\hat{p})}{\partial\boldsymbol{\Phi}_s} & \frac{\partial({}^n\hat{p})}{\partial\boldsymbol{\Phi}_m} & \frac{\partial({}^n\hat{p})}{\partial\boldsymbol{\Phi}_{ld}} \end{pmatrix}$$

$$= -\left\{\left[\frac{\partial({}^n R)}{\partial({}^{n-1}\hat{\mathbf{u}})} \frac{\partial({}^n R)}{\partial({}^{n-1}\hat{T})} \frac{\partial({}^n R)}{\partial({}^{n-1}\hat{p})}\right]\begin{pmatrix} \frac{\partial({}^{n-1}\hat{\mathbf{u}})}{\partial\boldsymbol{\Phi}_s} & \frac{\partial({}^{n-1}\hat{\mathbf{u}})}{\partial\boldsymbol{\Phi}_m} & \frac{\partial({}^{n-1}\hat{\mathbf{u}})}{\partial\boldsymbol{\Phi}_{ld}} \\ \frac{\partial({}^{n-1}\hat{T})}{\partial\boldsymbol{\Phi}_s} & \frac{\partial({}^{n-1}\hat{T})}{\partial\boldsymbol{\Phi}_m} & \frac{\partial({}^{n-1}\hat{T})}{\partial\boldsymbol{\Phi}_{ld}} \\ \frac{\partial({}^{n-1}\hat{p})}{\partial\boldsymbol{\Phi}_s} & \frac{\partial({}^{n-1}\hat{p})}{\partial\boldsymbol{\Phi}_m} & \frac{\partial({}^{n-1}\hat{p})}{\partial\boldsymbol{\Phi}_{ld}} \end{pmatrix} + \left[\frac{\partial({}^n R)}{\partial\boldsymbol{\Phi}_s} \quad \frac{\partial({}^n R)}{\partial\boldsymbol{\Phi}_m} \quad \frac{\partial({}^n R)}{\partial\boldsymbol{\Phi}_{ld}}\right]\right\}, \quad (24)$$

where we recall that

$$\left[\frac{\partial({}^n R)}{\partial({}^n\hat{\mathbf{u}})} \quad \frac{\partial({}^n R)}{\partial({}^n\hat{T})} \quad \frac{\partial({}^n R)}{\partial({}^n\hat{p})}\right]$$

is the tangent operator. (See Appendix II for detailed expressions.)

4. TURBULENT FLOW

To simplify this aspect of the analysis, we consider only isothermal turbulent flows described by the momentum and mass conservation equations.

For statistically stationary turbulent flow the pressure, velocity and body force can be expressed as the sum of a mean and a fluctuating part.[33] Following the usual procedure, the time-averaged forms of the momentum and mass conservation equations are written as

$$\begin{aligned} \rho[(\nabla_{\mathbf{x}}\tilde{\mathbf{u}})\tilde{\mathbf{u}}] &= -\nabla_{\mathbf{x}}\tilde{p} + \mathrm{div}_{\mathbf{x}}[2(\mu+\mu_t)\mathbf{D}(\tilde{\mathbf{u}})] + \rho\tilde{\mathbf{b}} \quad \text{in } b\times\mathscr{R}^N, \\ \mathrm{div}_{\mathbf{x}}(\tilde{\mathbf{u}}) &= 0 \quad \text{in } b\times\mathscr{R}^N, \end{aligned} \quad (25)$$

where μ_t is the eddy viscosity[24] and $\tilde{p} = \tilde{p} + \frac{2}{3}KE$ is redefined to include the eddy viscosity energy term (here KE denotes the kinetic energy). For clarity the overtildes (˜), which indicate the time-averages for $\mathbf{u}, p$ and $\mathbf{b}$, are omitted henceforth.

All that remains is to estimate μ_t. This is an active field of research. Most applications now use the k–ε model.[23] However, for very simple geometries a simpler model using a predetermined 'mixing length' can be employed with reasonable accuracy. In the mixing length model, μ_t is taken as[34]

$$\mu_t(l_m, \mathbf{D}) = \rho l_m^2[2\mathbf{D}(\mathbf{u})\cdot\mathbf{D}(\mathbf{u})]^{1/2}, \quad (26)$$

where l_m is defined by Nikuradse's formula[34] for circular cross-sections as

$$\frac{l_m}{r} = 0\cdot 14 - 0\cdot 08\left(1-\frac{y}{r}\right)^2 - 0\cdot 06\left(1-\frac{y}{r}\right)^4, \quad (27)$$

where r is the local radius in the tube and y is the distance from the wall.

Equation (25) is similar to the first and third equations of (15). However, in equation (25) the material properties are temperature-independent and the time-averaged flow quantities are used. Further, in equation (25) the turbulent viscosity μ_t is a function of the time-averaged rate-of-deformation tensor.

Following the same procedure as described in Section 3, we use the finite element and Newton–Raphson methods to solve equation (25) subject to the boundary conditions of equation (17) applied to the mean flow. The residual is defined in the reference configuration B as

$$R(\bar{\mathbf{u}}, \hat{p}) = \int_B \bar{\mathbf{u}} \cdot \hat{\rho}(\nabla_{\mathbf{X}} \hat{\mathbf{u}} \mathbf{J}^{-1} \hat{\mathbf{u}} - \hat{\mathbf{b}}) J \mathrm{d}v_{\mathbf{X}} + \int_B \{-\hat{p}\mathbf{I} \cdot \hat{\mathbf{D}}(\bar{\mathbf{u}}, \mathbf{J}) + \hat{\mathbf{D}}(\bar{\mathbf{u}}, \mathbf{J}) \cdot 2[(\mu + \hat{\mu}_t(\hat{l}_m, \hat{\mathbf{D}}))\hat{\mathbf{D}}(\hat{\mathbf{u}}, \mathbf{J})\} J \mathrm{d}v_{\mathbf{X}}$$
$$+ \int_B \bar{p}\mathbf{I} \cdot \hat{\mathbf{D}}(\hat{\mathbf{u}}, \mathbf{J}) J \mathrm{d}v_{\mathbf{X}} - \int_{A_t} \bar{\mathbf{u}} \cdot \hat{\mathbf{t}}^{\mathrm{p}} K \mathrm{d}a_{\mathbf{X}}$$
$$= 0, \tag{28}$$

where the $\hat{(\ )}$ quantities are as defined in Section 3 and

$$\hat{\mu}_t(\hat{l}_m, \hat{\mathbf{D}}) = \rho \hat{l}_m^2 [2\hat{\mathbf{D}}(\hat{\mathbf{u}}, \mathbf{J}) \cdot \hat{\mathbf{D}}(\hat{\mathbf{u}}, \mathbf{J})]^{1/2}. \tag{29}$$

By defining $\mathbf{U}(\boldsymbol{\Phi})$ as

$$\mathbf{U}(\boldsymbol{\Phi}) = (\hat{\mathbf{u}}(\boldsymbol{\Phi}), \hat{p}(\boldsymbol{\Phi})), \tag{30}$$

the tangent operator may be evaluated in partitioned form from

$$\frac{\partial R}{\partial \mathbf{U}} \mathrm{d}\mathbf{U} = \begin{pmatrix} \dfrac{\partial R}{\partial \hat{\mathbf{u}}} & \dfrac{\partial R}{\partial \hat{p}} \end{pmatrix} \begin{pmatrix} d\hat{\mathbf{u}} \\ d\hat{p} \end{pmatrix},$$

where the details appear in Appendix II.

4.1. Sensitivity analysis for the mixing length model

The sensitivity analysis follows from Section 3.2. For the turbulent flow problem the response function is expressed in the reference configuration as

$$G(\boldsymbol{\Phi}) = \int_B \hat{f}(\hat{\mathbf{u}}(\boldsymbol{\Phi}), \hat{\boldsymbol{\tau}}(\boldsymbol{\Phi}), \hat{\mathbf{D}}(\boldsymbol{\Phi}), \hat{p}(\boldsymbol{\Phi}), \boldsymbol{\Phi}) J(\boldsymbol{\Phi}) \mathrm{d}v_{\mathbf{X}} + \int_A \hat{h}(\hat{\mathbf{u}}(\boldsymbol{\Phi}), \hat{\mathbf{t}}(\boldsymbol{\Phi}), \boldsymbol{\Phi}) K(\boldsymbol{\Phi}) \mathrm{d}a_{\mathbf{X}}. \tag{31}$$

The design vector is still partitioned as shown in equation (23). The derivatives $\partial G/\partial \boldsymbol{\Phi}_s$, $\partial G/\partial \boldsymbol{\Phi}_m$, $\partial G/\partial \boldsymbol{\Phi}_{ld}$, $\partial G/\partial \hat{\mathbf{u}}$ and $\partial G/\partial \hat{p}$ are obtained directly from equations (45)–(48) and (50) respectively by eliminating all the temperature terms. The relations in equation (51) are also valid upon elimination of the temperature terms.

The response design derivatives

$$\frac{\partial \mathbf{U}}{\partial \boldsymbol{\Phi}} = \begin{pmatrix} \dfrac{\partial \hat{\mathbf{u}}}{\partial \boldsymbol{\Phi}_s} & \dfrac{\partial \hat{\mathbf{u}}}{\partial \boldsymbol{\Phi}_m} & \dfrac{\partial \hat{\mathbf{u}}}{\partial \boldsymbol{\Phi}_{ld}} \\ \dfrac{\partial \hat{p}}{\partial \boldsymbol{\Phi}_s} & \dfrac{\partial \hat{p}}{\partial \boldsymbol{\Phi}_m} & \dfrac{\partial \hat{p}}{\partial \boldsymbol{\Phi}_{ld}} \end{pmatrix}$$

are derived in a manner analogous to equation (24), while the residual sensitivities

$$\begin{bmatrix} \dfrac{\partial(^n R)}{\partial \boldsymbol{\Phi}_s} & \dfrac{\partial(^n R)}{\partial \boldsymbol{\Phi}_m} & \dfrac{\partial(^n R)}{\partial \boldsymbol{\Phi}_{ld}} \end{bmatrix}$$

(see equation (24)) are given in Appendix II.

5. EXAMPLE: LAMINAR FLOW IN AN AXISYMMETRIC CONTRACTION

In this example the finite element method, sensitivity analysis and numerical programming are combined to minimize the pressure drop in a steady, isothermal, laminar flow through an axisymmetric contraction. The density and viscosity are assumed constant and the body force **b** is independent of temperature T, so that the momentum and mass conservation equations may be analysed prior to the energy conservation equation. In fact, only the momentum and mass conservation equations are solved for the optimization. However, all equations are included in the sensitivity verification.

5.1. Analysis

The axisymmetric contraction studied appears in Figure 1. Dimensionless variables are used so that the scaled values of the inlet radius r_i, outlet radius r_o, contraction length L_2, inlet length L_1 and outlet length L_3 are chosen as $r_i/L_1 = 1{\cdot}2, r_o/L_1 = 0{\cdot}24, L_2/L_1 = 4{\cdot}0$ and $L_3/L_1 = 2{\cdot}4$ and remain unchanged throughout the optimization.

An axial velocity profile, which defines the flow rate, is prescribed on the inlet end ($z = 0$). The dimensionless boundary conditions are

$$\begin{aligned} u_z &= 1 - r^2/r_i^2 \quad \text{at } z = 0, \\ u_r &= 0 \quad \text{at } z = 0, \\ u_z = u_r &= 0 \quad \text{on } A_w, \\ u_r &= 0 \quad \text{at } r = 0, \\ t_z^p &= 0 \quad \text{at } r = 0, \\ p &= 0 \quad \text{at } z = L_1 + L_2 + L_3, \\ u_r &= 0 \quad \text{at } z = L_1 + L_2 + L_3, \end{aligned} \tag{32}$$

where A_w is the contraction wall identified by the hash marking in Figure 1. Dimensionless variables defined by $\mathbf{u}^* = \mathbf{u}/u_{z\max}$, $\mathbf{x}^* = \mathbf{x}/2r_i$ and $p^* = p/\rho u_{z\max}^2$ have been introduced, where $u_{z\max} = u_z$ at $r = 0, z = 0$ and the (*) has been dropped. The upstream condition on u_z corresponds to fully developed flow in the inlet section. The Reynolds number is defined as $Re = 2\rho r_i u_{z_{\max}}/\mu$, which we take to be 28·8. The effect of flow rate can be examined by varying the Reynolds number.

The contraction inlet and outlet extensions are included to ensure that the incoming flow is independent of the contraction and the flow is fully developed at the pipe exit ($z = L_1 + L_2 + L_3$). We also performed a finite element mesh convergence study for this example and found that a finite element mesh consisting of 2565 nodes and 2380 isoparametric quadrilateral elements with bilinear

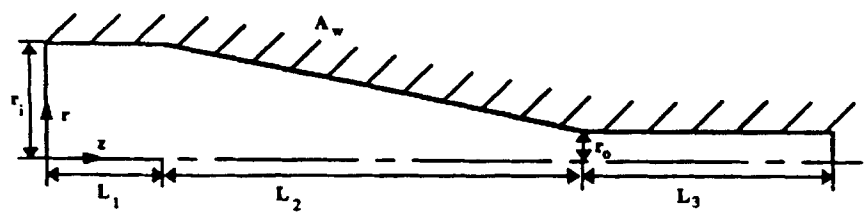

Figure 1. Initial contraction design (not drawn to scale)

velocity and constant pressure interpolation is adequate. It is well known that this interpolation scheme may yield spurious pressure oscillations, which are most often observed in continuity-driven flows. No oscillations were found in our solutions.*

5.2. *Optimization*

The optimization seeks to minimize the pressure drop across the contraction by modifying the shape in the transition region (see Figure 1). The design parameter vector $\mathbf{\Phi} = (\Phi_1, \Phi_2, \ldots, \Phi_{12})$ is used to define the radial co-ordinates of the mesh control points (see Figure 2). A cubic spline passes through each adjacent pair of control points. The spline and mesh are created via the PATRAN programme[36] and we ensure that the slope is continuous between the adjacent spline segments.[36]

In addition, zero-slope conditions are imposed on the geometry at the inlet and outlet ends of the transition region. Standard mapped meshing techniques are then used to interpolate the mesh node co-ordinates x^I from the spline using the same PATRAN preprocessor. To evaluate the node co-ordinate sensitivities $\partial x^I / \partial \Phi_i$ required for the shape sensitivity analysis, we use a PATRAN PCL programme.[37]

The cost function of the optimization problem is the pressure drop across the contraction, which is expressed over the reference configuration as

$$G = \int_{A_i} \hat{p} K r \, da_{\mathbf{X}} - \int_{A_m} \hat{p} K r \, da_{\mathbf{X}}, \tag{33}$$

where A_i and A_m are the cross-sections located at the inlet and outlet ends of the contraction respectively (see Figure 2) and the appropriate modifications for the axisymmetric description are applied to equation (22).[38] The sensitivities of the response function are obtained by differentiation of equation (33):

$$\frac{\partial G}{\partial \Phi_i} = \int_{A_i} \left(\frac{\partial \hat{p}}{\partial \Phi_i} K r + \hat{p} \frac{\partial (K r)}{\partial \Phi_i} \right) da_{\mathbf{X}} - \int_{A_m} \left(\frac{\partial \hat{p}}{\partial \Phi_i} K r + \hat{p} \frac{\partial (K r)}{\partial \Phi_i} \right) da_{\mathbf{X}}, \tag{34}$$

where it is noted that $\partial (Kr)/\partial \Phi_i = 0$ for this example since the radii of the inlet and outlet are fixed.

In the following we discuss a preliminary sensitivity analysis and then the optimization results. The finite element analyses and direct differentiation shape sensitivities are computed with an enhanced version of FIDAP[39] and the optimizations are performed with DOT[40] using the Broydon–Fletcher–Goldfarb–Shanno (BFGS) algorithm.[41]

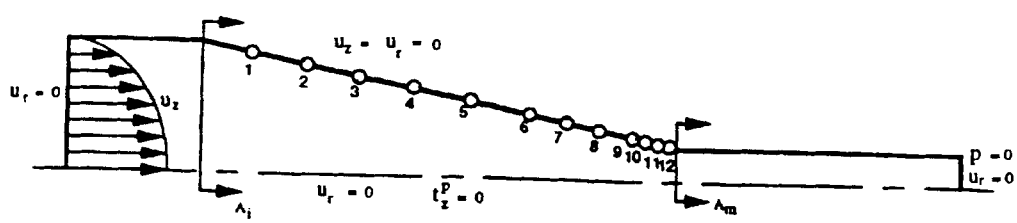

Figure 2. Boundary conditions and design parameter distribution (not drawn to scale)

* Supporting studies for the adequacy of the extensions, mesh and pressure interpolations appear in Reference 35.

5.2.1. Sensitivity results. Sensitivities play an important role in the optimization. Before commencing the optimization, a sensitivity analysis is performed on the initial design to illustrate the usefulness of the sensitivity analysis and to verify the accuracy of the direct differentiation sensitivity computations.

The response sensitivities are calculated for the weakly coupled thermal–fluid problem. The thermal boundary conditions are defined as

$$\begin{aligned} T &= 298\ \text{K} \quad \text{at } z = 0, \\ q^s &= h(T - 293\text{K}) \quad \text{on } A_w, \\ q^s &= 0 \quad \text{at } z = L_1 + L_2 + L_3, \\ q^s &= 0 \quad \text{at } r = 0, \end{aligned} \tag{35}$$

where $h = 40\ \text{W m}^{-2}\ \text{K}^{-1}$ and the boundary conditions of equation (32) still apply.

The pressure drop sensitivities (see equation (34)) are plotted in Figure 3. Note that all the sensitivity values are negative. Therefore an increase in each design parameter value (i.e. increasing the radius) will reduce the pressure drop. Also note that the sensitivities are not monotonic. For example, $|\partial p/\partial \Phi_9| > |p/\partial \Phi_{10}|$. One reason for this is that the amount of surface area affected by the design parameters is not equal. For example, a perturbation of Φ_9 displaces the contraction more than an equal perturbation of Φ_{10}. This figure illustrates how sensitivity analysis can be used in its own right, e.g. for trade-off studies and to gain insight into the flow system.

The response sensitivities $\partial p/\partial \Phi_1$ are depicted in Figure 4.* As expected, significant sensitivity values exist only in the neighbourhood of Φ_1, while the sensitivities are very small or zero in all other regions. Similar observations can be made about other design parameters.

To validate the direct differentiation sensitivity evaluations, we also compute sensitivities by the central finite difference method.[28] It is emphasized that for each design parameter, two additional finite element meshes are generated and two additional finite element analyses are performed to obtain the central finite difference sensitivities. When the number of design parameters is large, this finite difference method proves to be computationally prohibitive. Furthermore, round-off or truncation errors may adversely affect the results,[28] which is particularly an issue here, as the PATRAN PCL programme which is used to generate the finite element mesh is single-precision.

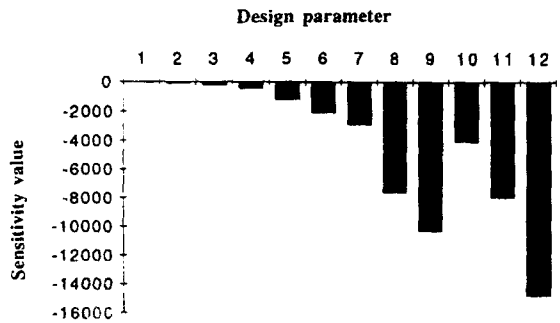

Figure 3. Pressure drop sensitivities for initial contraction shape

* Similar plots for $\partial \mathbf{u}_z/\partial \Phi_1$, $\partial \mathbf{u}_r/\partial_1$, and $\partial T/\partial \Phi_1$ appear in Reference 35.

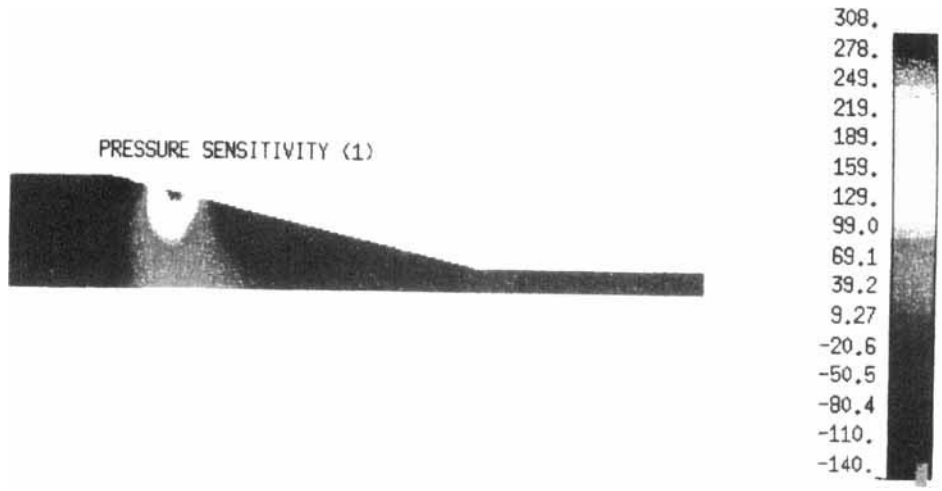

Figure 4. Sensitivity $\partial p/\partial \Phi_1$

The direct differentiation and finite difference pressure drop sensitivities, i.e. $\partial G/\partial \Phi_i$ ($i = 1, \ldots, 12$), are compared in Table I. In all cases the discrepancy between the two results is small (less than 0·02%), thus verifying the accuracy of the efficiently computed direct differentiation sensitivities.

5.2.2. Shape optimization. In this optimization we minimize the pressure drop (see equation (33)) subject to the side constraints that the design parameters (i.e. radii) do not exceed the inlet radius (see Table II).

The optimization requires 31 iterations (where sensitivities are performed) and 135 analyses (for the one-dimensional searches). The net pressure drop is reduced by 3·9% from 57,138 to 54,888. Most design parameter values attain their upper bounds in the optimal design. The initial and optimal contraction designs are denoted in Table II and illustrated in Figure 5.

The pressure along the z-axis ($r = 0$) for the initial and optimal designs appears in Figure 6. Since the inlet pressure is nearly uniform at the entrance, it is clear that the pressure in the optimal design is lower at the inlet end ($z = 1$) and higher at the end of the contraction ($z = 5$) than that of the initial design, thus yielding a lower pressure drop across the contraction.

Table I. Design sensitivity $\partial G/\partial \Phi_i$ for initial design using direct differentiation and finite difference methods

Design parameter	Direct differentiation	Finite difference	Discrepancy (%)
1	−50·9974	−51·0078	$-2{\cdot}03 \times 10^{-2}$
2	−104·8415	−104·8306	$1{\cdot}04 \times 10^{-2}$
3	−201·9189	−201·8817	$1{\cdot}84 \times 10^{-2}$
4	−425·2562	−425·1591	$2{\cdot}28 \times 10^{-2}$
5	−1195·4892	−1195·5578	$-5{\cdot}74 \times 10^{-3}$
6	−2104·2595	−2104·1294	$6{\cdot}18 \times 10^{-3}$
7	−2903·6879	−2903·5867	$3{\cdot}48 \times 10^{-3}$
8	−7595·8226	7596·2845	$-6{\cdot}08 \times 10^{-3}$
9	−10286·4281	−10286·7772	$-3{\cdot}39 \times 10^{-3}$
10	−4070·3855	−4070·6254	$-5{\cdot}89 \times 10^{-3}$
11	−7949·7037	−7948·3413	$1{\cdot}71 \times 10^{-2}$
12	−14805·5955	−14807·7171	$-1{\cdot}43 \times 10^{-2}$

Table II. Initial and optimal design parameter values. Active side constraints are marked with an asterisk

Design parameter	Initial value	Upper bound	Lower bound	Optimal value
1	1·080	1·200	0·800	1·2000*
2	0·960	1·200	0·800	1·2000*
3	0·840	1·200	0·600	1·2000*
4	0·720	1·200	0·600	1·2000*
5	0·600	1·200	0·450	1·2000*
6	0·480	1·200	0·300	1·2000*
7	0·420	1·200	0·200	1·0808
8	0·360	1·200	0·200	0·8116
9	0·300	1·200	0·200	0·4918
10	0·285	1·200	0·150	0·4175
11	0·270	1·200	0·150	0·3410
12	0·255	1·200	0·150	0·3019

The pressure drop reduction is related to reducing the friction loss through the contraction, which comes from the shear stress acting tangent to the contraction wall. Figure 7 illustrates the tangent shear stress distributions for the initial and optimal designs. Upon comparing the two distributions, it is seen that the tangent shear stress in the optimal design is significantly less over most of the contraction; however, the tangent shear stress is higher in a small portion of the contraction. In the outlet extensions, the tangent shear stress distributions along the wall are almost identical for the two designs. Note that the tangent shear stress decreases slightly at the beginning of the contraction for both designs. These decreases are due to the velocity changes caused by the contraction. Durst and Loy observed a similar phenomena for a pipe with an abrupt contraction.[42]

The Kuhn–Tucker conditions[43,44] requires that the sensitivities $\partial G/\partial \Phi_i$ vanish at the optimal design if the side constraint (i.e. the upper or lower bound) associated with design parameter Φ_i is not active. The sensitivities for the initial and optimal designs are denoted in Table III. Using these sensitivities and the optimal parameter values listed in Table II, we note that the sensitivities associated with the non-active side constraints conform to the Kuhn–Tucker conditions to within a tolerance of 0·15% of the initial sensitivity value.

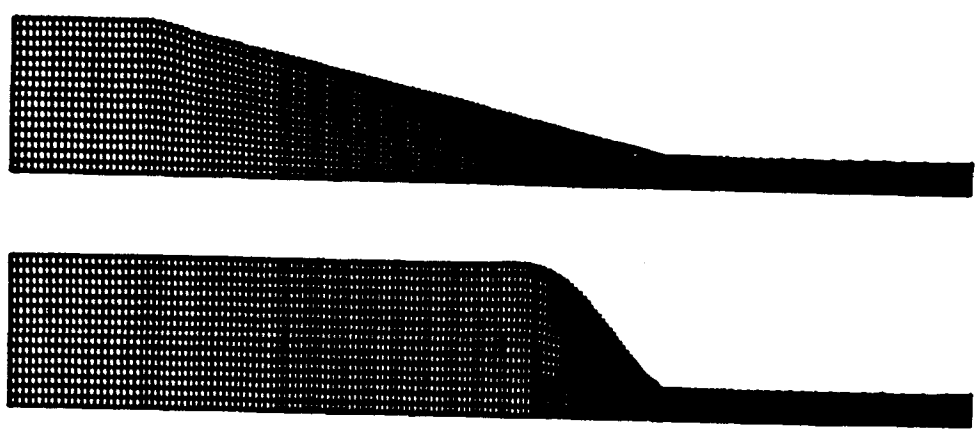

Figure 5. Initial and optimal contraction shapes

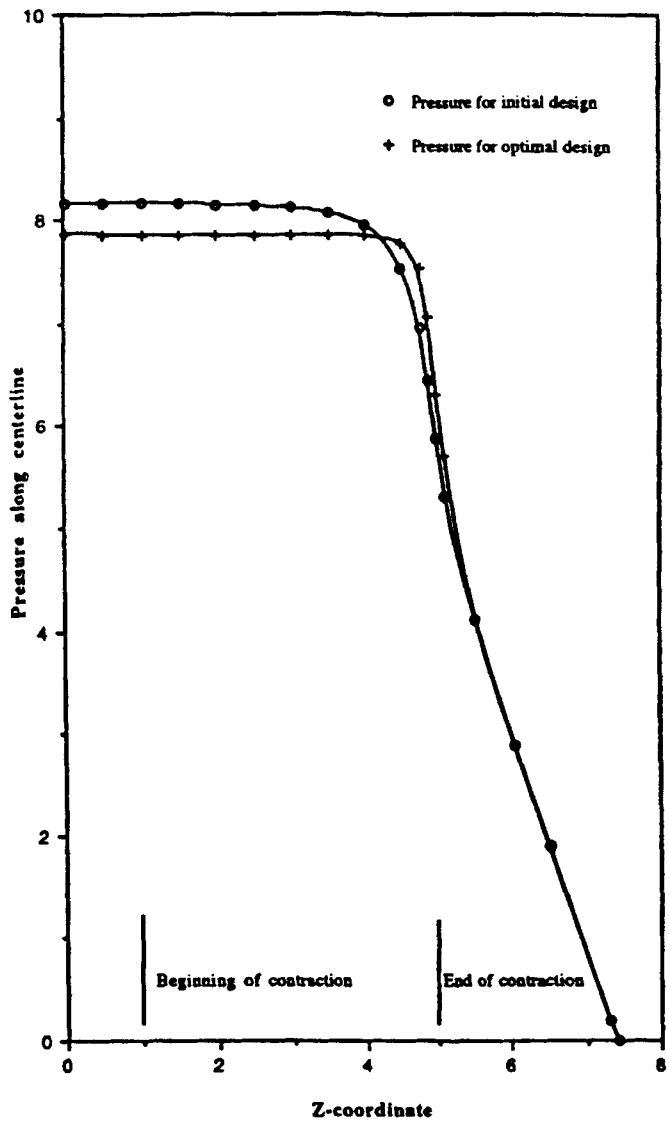

Figure 6. Pressure along z-axis for initial and optimal designs

6. EXAMPLE: TURBULENT FLOW IN AN AXISYMMETRIC CONTRACTION

In the previous section the cross-section of an axisymmetric contraction is optimized for a low-Reynolds-number laminar flow. The problem is now repeated with a high-Reynolds-number turbulent flow. Consequently, this analysis uses the mixing length turbulence model and the time-averaged momentum and mass conservation equations. All material properties are constant and temperature-independent.

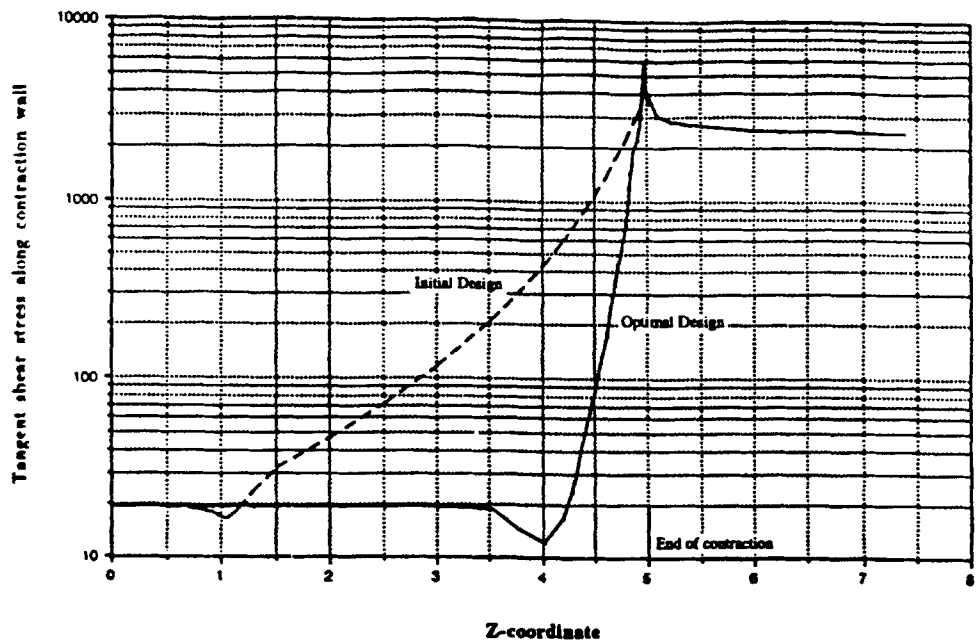

Figure 7. Tangent shear stress along contraction wall for initial and optimal designs

6.1. Problem statement

The axisymmetric contraction shape illustrated in Figure 1 is optimized. However, in this example the dimensions are chosen so that $r_i/L_1 = 0 \cdot 5, r_o/L_1 = 0 \cdot 2, L_2/L_1 = 3 \cdot 5$ and $L_3/L_1 = 1 \cdot 5$ and the boundary condition of the first equation of (32) is replaced with a constant axial velocity profile boundary condition $u_z = 1$, except at $r = r_i$ where $u_z = 0$. The longer inlet region is chosen so that the incoming flow may become fully developed and hence the mixing length model can be used to simulate the response.

Table III. Sensitivities for initial and optimal designs and their ratio. An asterisk denotes optimal sensitivities with respect to active side constraints

Design parameter	Sensitivity (initial design)	Sensitivity (optimal design)	Optimal sens. / Initial sens.
1	−51·00	−37·36*	0·73*
2	−104·8	−38·92*	0·37*
3	−201·9	−37·94*	0·19*
4	−425·2	−34·92*	$8{\cdot}21 \times 10^{-2}$*
5	−1195	−24·09*	$2{\cdot}02 \times 10^{-2}$*
6	−2104	−3·704*	$1{\cdot}76 \times 10^{-3}$*
7	−2904	−0·798	$2{\cdot}75 \times 10^{-4}$
8	−7596	0·3441	$4{\cdot}53 \times 10^{-5}$
9	−10286	−2·071	$2{\cdot}01 \times 10^{-4}$
10	−4070	−0·218	$5{\cdot}36 \times 10^{-5}$
11	−7950	12·04	$1{\cdot}51 \times 10^{-3}$
12	−14806	−6·671	$4{\cdot}51 \times 10^{-4}$

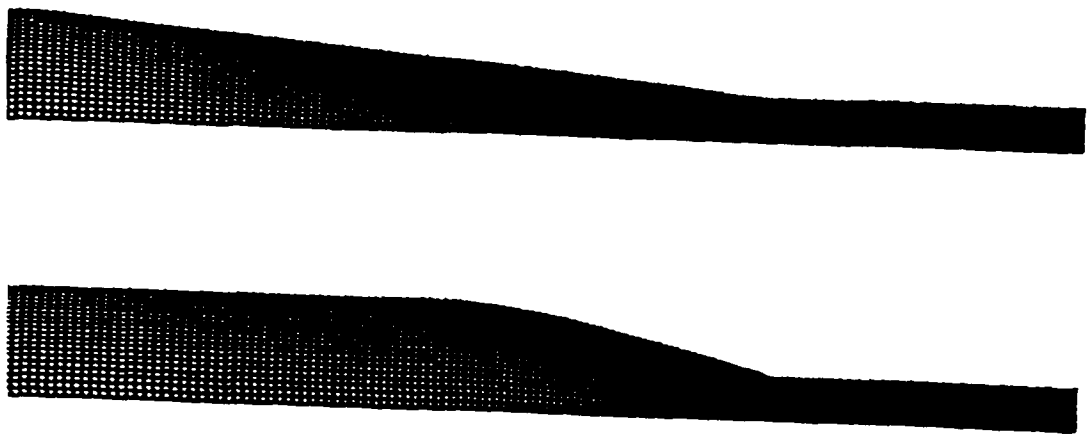

Figure 8. Initial and optimal contraction shapes

The Reynolds number $Re = \rho \bar{u} L/\mu$ is chosen as 2×10^4. This value is low enough so that the numerical instabilities common to flow problems which require upwinding stabilization techniques do not appear in the present calculations. For this example the turbulent viscosity μ_t is signficantly greater than molecular viscosity μ. This mesh uses 2814 isoparametric quadrilateral elements which employ bilinear velocity and constant pressure interpolation. We use nine design parameters to parametrize the shape of the contraction, as illustrated in Figure 8.

6.2. Contraction optimization

Before commencing the optimization, the pressure drop sensitivities $\partial G/\partial \Phi_i$ $(i = 1, \ldots, 9)$ are calculated for the initial design by both the direct differentiation and finite difference methods. Comparisons between these two computations[35] confirm that the efficiently computer direct differentiation sensitivities are correct.

The design optimization converges in 15 iterations. The initial and optimal contraction shapes appear in Figure 8 and the initial, optimal, upper-bound and lower-bound values for the design parameters are denoted in Table IV. The optimization requires 15 sensitivity analyses and 63 analyses (for the one-dimensional searches).

Table IV. Initial and optimal design parameter values for turbulent flow optimization. Active side constraints are marked with an asterisk

Design parameter	Initial value	Upper bound	Lower bound	Optimal value
1	0·4571	0·500	0·355	0·5000*
2	0·4143	0·500	0·205	0·5000*
3	0·3714	0·500	0·203	0·5000*
4	0·3286	0·500	0·203	0·4999
5	0·2857	0·500	0·203	0·4394
6	0·2429	0·500	0·203	0·3317
7	0·2214	0·500	0·203	0·2691
8	0·2107	0·500	0·200	0·2357
9	0·2054	0·500	0·200	0·2197

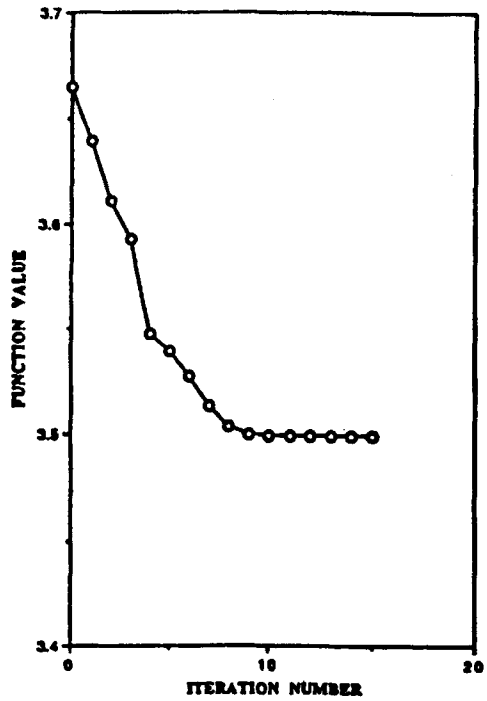

Figure 9. Cost function history for turbulent flow optimization

Comparing this optimal contraction shape with that in the previous example, we see that this optimal design has a more gradual taper. The cost function (i.e. the net pressure drop) history (see Figure 9) shows that the optimization converges rapidly over the first nine iterations; thereafter the cost function value changes only slightly. The optimal design yields a 4·5% net pressure drop reduction compared with the initial design.

The design sensitivities $\partial G/\partial \Phi_i$ $(i = 1, \ldots, 9)$ for the initial and optimal designs are shown in Table V. The sensitivities related to the non-active side constraint design parameters are approximately zero for the optimal design, indicating that the Kuhn–Tucker conditions are satisfied.

Table V. Sensitivities for initial and optimal designs and their ratio. An asterisk denotes optimal sensitivities with respect to active side constraints

Design parameter	Sensitivity (initial design)	Sensitivity (optomal design)	Optimal sens / Initial sens.
1	− 0·06601	− 0·05306*	$8{\cdot}04 \times 10^{-1}$*
2	− 0·05796	− 0·02496*	$4{\cdot}31 \times 10^{-1}$*
3	− 0·1181	− 0·02514*	$2{\cdot}13 \times 10^{-1}$*
4	− 0,2549	$-3{\cdot}179 \times 10^{-4}$	$1{\cdot}25 \times 10^{-3}$
5	− 0,7317	$-8{\cdot}438 \times 10^{-4}$	$1{\cdot}15 \times 10^{-3}$
6	− 1·3802	$-1{\cdot}204 \times 10^{-3}$	$8{\cdot}72 \times 10^{-4}$
7	− 1·3488	$1{\cdot}928 \times 10^{-5}$	$1{\cdot}43 \times 10^{-5}$
8	− 0·9184	$-6{\cdot}570 \times 10^{-3}$	$7{\cdot}15 \times 10^{-3}$
9	− 2·2082	$-2{\cdot}469 \times 10^{-3}$	$1{\cdot}12 \times 10^{-3}$

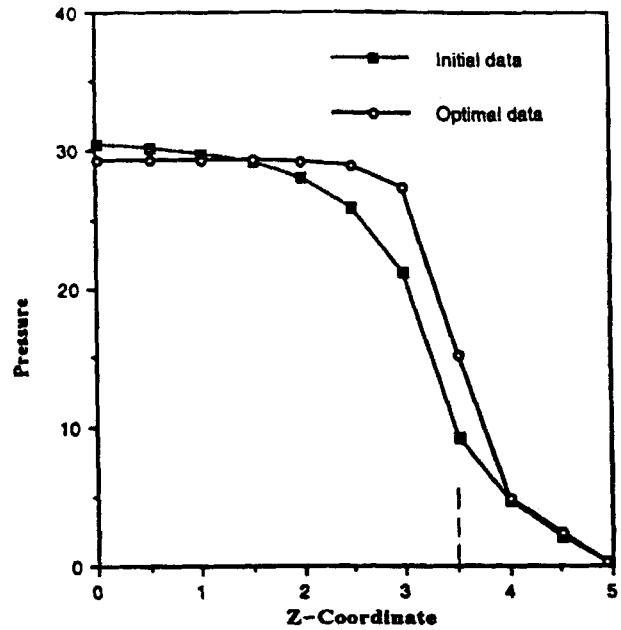

Figure 10. Pressure along z-axis for initial and optimal designs

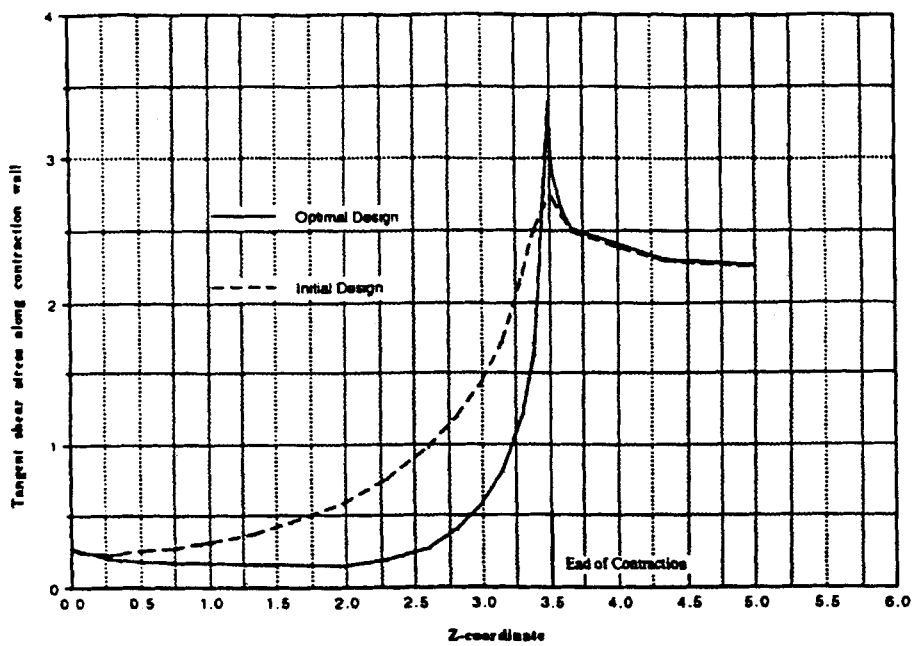

Figure 11. Tangent shear stress distribution for initial and optimal designs

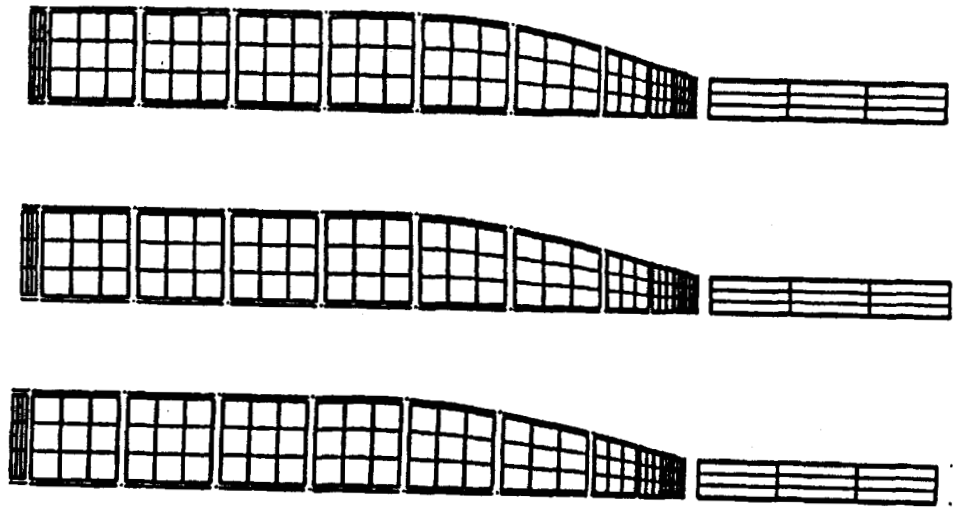

Figure 12. Optimal contraction shapes for $Re = 5 \times 10^3$, 2×10^4 and 2×10^5

The time-averaged pressure contours along the z-axis ($r = 0$) for the initial and optimal designs appear in Figure 10. It is clear from this figure that the pressure drop along the centreline in the optimal design is reduced across the contraction. Again the friction loss is related to the tangent shear stress acting along the contraction wall and again the reduction of the tangent shear stress due to the optimization is evident (see Figure 11). However, in turbulent flow the high-shear-stress region is confined to the boundary layer near the wall; this localization accounts for the differences between the laminar and turbulent optimal designs.

Shape optimizations are also performed for Reynolds numbers $Re = 5 \times 10^3$ and 2×10^5. The optimal designs for all three Reynolds numbers are illustrated in Figure 12. As seen from the figure, these three optimal shapes are almost identical. This shows that for this contraction and turbulence model, the optimal design is relatively insensitive to the Reynolds number and further confirms the notion that the high shear stress is confined to the boundary layer.

7. DISCUSSION AND CONCLUSIONS

A systematic design approach is presented for transient non-linear coupled flow and turbulent flow systems. The design sensitivities of a generalized response functional are computed via the direct differentiation method with respect to shape, material property and load data parameters. The efficiently computed sensitivities are combined with numerical optimization to form a computer-aided optimal design environment. Finally, this optimization algorithm is used to minimize the pressure drop for both laminar and turbulent flows through contractions.

We note that the sensitivity terms such as $\partial \mathbf{R}/\partial \Phi_i$ in equation (9) may be tedious to encode. Therefore it may be expedient to utilize automatic differentiation[45] to hasten the software development. However, we do not recommend a black box approach to automatic differentiation sensitivity analysis, as this approach does not utilize the decomposed tangent operator and therefore the final code is not nearly as computationally efficient as the direct differentiation method. In fact, Bischof *et al.*[45] give examples where the black box automatic differentiation sensitivity calculations actually require more computational time than the non-linear primal analysis.

It is well known that the wall shear stress for laminar flow increases as the pipe diameter decreases. Hence the laminar flow optimization generated a design in which the cross-sectional area remained

large over a majority of the contraction region. However, this laminar design should not be used for a turbulent flow, as recirculation would otherwise arise in the abruptly tapered region. Therefore the turbulent design exhibits a more gradual taper. This design minimizes the wall surface area, thereby reducing the net friction loss through the contraction.

The sensitivity formulations are derived for the transient thermal–flow coupled systems. As further applications, design optimizations may be performed for tranisent coupled problems. These optimizations can be performed for shape changes as well as material property, boundary condition, initial condition and load data variations.

ACKNOWLEDGEMENT

This work is supported by the National Science Foundation (Grant DDM 92-15599) and NASA (Grant NAG 3-1286).

APPENDIX I: SENSITIVITY ANALYSIS FOR A PENALTY METHOD

The penalty method is frequently used to analyse the previous problem rather than the mixed formulation.[46] In the penalty method the pressure is eliminated and the momentum and energy conservation equations are expressed solely in terms of the velocity and temperature fields by introducing a penalty formulation for the mass conservation equation. The sensitivities for the velocity and temperature fields are then obtained directly. However, the pressure sensitivities require additional computations.

In the penalty method an artificial compressibility is added as a penalty term on the right side of the mass conservation equation (third equation of (15)):

$$\mathrm{div}_{\mathbf{x}}(\mathbf{u}) = -\epsilon p, \tag{36}$$

where the penalty parameter ε is sufficiently small to obtain accurate analysis results. The advantage of this method is that it reduces the number of equations in finite element applications.

Equation (36) is transformed to the reference configuration and then substituted into equation (19) to yield

$$\begin{aligned} R(\hat{\mathbf{u}}, \hat{T}) = 0 = &\int_B \bar{\mathbf{u}} \cdot \hat{\rho}\left(\frac{\partial \hat{\mathbf{u}}}{\partial t} + \nabla_{\mathbf{X}}\hat{\mathbf{u}}^{-1}\hat{\mathbf{u}} - \hat{\mathbf{b}}\right) J \mathrm{d}v_{\mathbf{X}} \\ &+ \int_B \left(\frac{1}{\epsilon}\mathrm{div}_{\mathbf{X}}(J\mathbf{J}^{-1}\hat{\mathbf{u}}) \cdot \hat{\mathbf{D}}(\bar{\mathbf{u}}, \mathbf{J})\right) \mathrm{d}v_{\mathbf{X}} \\ &+ \int_B [\hat{\mathbf{D}}(\bar{\mathbf{u}}, \mathbf{J}) \cdot 2\hat{\mu}\hat{\mathbf{D}}(\hat{\mathbf{u}}, \mathbf{J})] J \mathrm{d}v_{\mathbf{X}} \\ &+ \int_B \bar{T}\hat{\rho}\left(\frac{\partial \hat{e}}{\partial t} + \hat{\mathbf{u}} \cdot \mathbf{J}^{-\mathrm{T}}\nabla_{\mathbf{X}}\hat{e} - \hat{\mathbf{Q}}\right) J \mathrm{d}v_{\mathbf{X}} \\ &- \int_B \left(\bar{T}\hat{\mathbf{D}}(\hat{\mathbf{u}}, \mathbf{J}) \cdot \frac{1}{\epsilon}\mathrm{div}_{\mathbf{X}}(J\mathbf{J}^{-1}\hat{\mathbf{u}})\right) \mathrm{d}v_{\mathbf{X}} \\ &- \int_B [\bar{T}\hat{\mathbf{D}}(\hat{\mathbf{u}}, \mathbf{J}) \cdot 2\hat{\mu}\hat{\mathbf{D}}(\hat{\mathbf{u}}, \mathbf{J})] J \mathrm{d}v_{\mathbf{X}} \\ &+ \int_B \hat{\mathbf{g}}(\bar{T}, \mathbf{J}) \cdot \hat{\mathbf{k}}\hat{\mathbf{g}}(\hat{T}, \mathbf{J}) J \mathrm{d}v_{\mathbf{X}} + \int_{A_q} \bar{T}\hat{q}^{\mathrm{p}} K \mathrm{d}a_{\mathbf{X}} \\ &- \int_{A_t} \bar{\mathbf{u}} \cdot \hat{\mathbf{t}}^{\mathrm{p}} K \mathrm{d}a_{\mathbf{X}}. \end{aligned} \tag{37}$$

The referential pressure $\hat{p}$ is eliminated from the residual, so that all terms involving pressure are neglected in equation (24) and equations (42) and (55) become

$$\begin{aligned}\frac{\partial({}^nR)}{\partial({}^n\hat{\mathbf{u}})}\mathrm{d}\hat{\mathbf{u}} = &\int_B \bar{\mathbf{u}}\cdot\hat{\rho}\left(\frac{\mathrm{d}\hat{\mathbf{u}}}{\Delta t}+\nabla_{\mathbf{X}}{}^n\hat{\mathbf{u}}\mathbf{J}^{-1}\mathrm{d}\hat{\mathbf{u}}+\nabla_{\mathbf{X}}\mathrm{d}\hat{\mathbf{u}}\mathbf{J}^{-1}{}^n\hat{\mathbf{u}}\right)J\mathrm{d}v_{\mathbf{X}}\\
&+\int_B[\hat{\mathbf{D}}(\bar{\mathbf{u}},\mathbf{J})\cdot 2\hat{\mu}\hat{\mathbf{D}}(\mathrm{d}\hat{\mathbf{u}}\mathbf{J})]J\mathrm{d}v_{\mathbf{X}}\\
&+\int_B \bar{T}[\hat{\rho}\mathrm{d}\hat{\mathbf{u}}\cdot\mathbf{J}^{-\mathrm{T}}\nabla_{\mathbf{X}}{}^n\hat{e}-\hat{\mathbf{D}}({}^n\hat{\mathbf{u}},\mathbf{J})\cdot 4\hat{\mu}\hat{\mathbf{D}}(\mathrm{d}\hat{\mathbf{u}},\mathbf{J})]J\mathrm{d}v_{\mathbf{X}}\\
&+\int_B\left(\frac{1}{\epsilon}\mathrm{div}_{\mathbf{X}}(J\mathbf{J}^{-1}\mathrm{d}\hat{\mathbf{u}})\cdot\hat{\mathbf{D}}(\bar{\mathbf{u}},\mathbf{J})\right)\mathrm{d}v_{\mathbf{X}}\\
&-\int_B \bar{T}\frac{1}{\epsilon}[\mathrm{div}_{\mathbf{X}}(J\mathbf{J}^{-1}\mathrm{d}\hat{\mathbf{u}})\cdot\hat{\mathbf{D}}({}^n\hat{\mathbf{u}},\mathbf{J})\\
&+\mathrm{div}_{\mathbf{X}}(J\mathbf{J}^{-1}{}^n\hat{\mathbf{u}})\cdot\hat{\mathbf{D}}(\mathrm{d}\hat{\mathbf{u}},\mathbf{J})]\mathrm{d}v_{\mathbf{X}},\end{aligned}\tag{38}$$

$$\begin{aligned}\frac{\partial({}^nR)}{\partial\boldsymbol{\Phi}_{\mathrm{s}}} = &\int_B\Bigg[\bar{\mathbf{u}}\cdot\hat{\rho}\left(\frac{{}^n\hat{\mathbf{u}}-{}^{n-1}\hat{\mathbf{u}}}{\Delta t}+\nabla_{\mathbf{X}}{}^n\hat{\mathbf{u}}\mathbf{J}^{-1}{}^n\hat{\mathbf{u}}-{}^n\hat{\mathbf{b}}\right)\\
&+\hat{\mathbf{D}}(\bar{\mathbf{u}},\mathbf{J})\cdot 2\hat{\mu}\hat{\mathbf{D}}({}^n\hat{\mathbf{u}},\mathbf{J})\Bigg]\frac{\partial J}{\partial\boldsymbol{\Phi}_{\mathrm{s}}}\mathrm{d}v_{\mathbf{X}}\\
&-\int_{A_t}\bar{\mathbf{u}}\cdot\hat{\mathbf{t}}^{\mathrm{p}}\frac{\partial K}{\partial\boldsymbol{\Phi}_{\mathrm{s}}}\mathrm{d}a_{\mathbf{X}}+\int_B\bar{\mathbf{u}}\cdot\hat{\rho}\left(\nabla_{\mathbf{X}}{}^n\hat{\mathbf{u}}\frac{\partial\mathbf{J}^{-1}}{\boldsymbol{\Phi}_{\mathrm{s}}}{}^n\hat{\mathbf{u}}\right)J\mathrm{d}v_{\mathbf{X}}\\
&+\int_B\left[\hat{\mathbf{D}}\left(\bar{\mathbf{u}},\frac{\partial\mathbf{J}}{\partial\boldsymbol{\Phi}_{\mathrm{s}}}\right)\cdot 2\hat{\mu}\hat{\mathbf{D}}({}^n\hat{\mathbf{u}},\mathbf{J})+\hat{\mathbf{D}}(\bar{\mathbf{u}},\mathbf{J})\cdot 2\hat{\mu}\hat{\mathbf{D}}\left({}^n\hat{\mathbf{u}},\frac{\partial\mathbf{J}}{\partial\boldsymbol{\Phi}_{\mathrm{s}}}\right)\right]J\mathrm{d}v_{\mathbf{X}}\\
&+\int_B\bar{T}\hat{\rho}\left(\frac{{}^n\hat{e}-{}^{n-1}\hat{e}}{\Delta t}+{}^n\hat{\mathbf{u}}\cdot J^{-\mathrm{T}}\nabla_{\mathbf{X}}{}^n\hat{e}-{}^n\hat{Q}\right)\frac{\partial J}{\partial\boldsymbol{\Phi}_{\mathrm{s}}}\mathrm{d}v_{\mathbf{X}}\\
&+\int_B[\hat{g}(\bar{T},\mathbf{J})\cdot\hat{\mathbf{k}}\hat{\mathbf{g}}({}^n\hat{T},\mathbf{J})]\frac{\partial J}{\partial\boldsymbol{\Phi}_{\mathrm{s}}}\mathrm{d}v_{\mathbf{X}}+\int_{A_q}\bar{T}\hat{q}^{\mathrm{p}}\frac{\partial K}{\partial\boldsymbol{\Phi}_{\mathrm{s}}}\mathrm{d}a_{\mathbf{X}}\\
&-\int_B\hat{T}\left(\hat{\mathbf{D}}({}^n\hat{\mathbf{u}},\mathbf{J})\cdot 2\mu\hat{\mathbf{D}}({}^n\hat{\mathbf{u}},\mathbf{J})\frac{\partial J}{\partial\boldsymbol{\Phi}_{\mathrm{s}}}\right)\mathrm{d}v_{\mathbf{X}}\\
&+\int_B\bar{T}\hat{\rho}\left({}^n\hat{\mathbf{u}}\cdot\frac{\partial\mathbf{J}^{-\mathrm{T}}}{\partial\boldsymbol{\Phi}_{\mathrm{s}}}\nabla_{\mathbf{X}}{}^n\hat{e}\right)J\mathrm{d}v_{\mathbf{X}}\\
&+\int_B\frac{1}{\epsilon}\Bigg[\mathrm{div}_{\mathbf{X}}(J\mathbf{J}^{-1}{}^n\hat{\mathbf{u}})\cdot\hat{\mathbf{D}}\left(\bar{\mathbf{u}},\frac{\partial\mathbf{J}}{\partial\boldsymbol{\Phi}_{\mathrm{s}}}\right)+\mathrm{div}_{\mathbf{X}}\left(J\frac{\partial\mathbf{J}^{-1}{}^n}{\partial\boldsymbol{\Phi}_{\mathrm{s}}}\hat{\mathbf{u}}\right)\cdot\hat{\mathbf{D}}(\bar{\mathbf{u}},\mathbf{J})\\
&+\mathrm{div}_{\mathbf{X}}\left(\frac{\partial J}{\partial\boldsymbol{\Phi}_{\mathrm{s}}}\mathbf{J}^{-1}{}^n\hat{\mathbf{u}}\right)\cdot\hat{\mathbf{D}}(\bar{\mathbf{u}},\mathbf{J})\Bigg]\mathrm{d}v_{\mathbf{X}}\\
&-\int_{B_{\mathbf{X}}}\bar{T}\frac{1}{\epsilon}\Bigg[\mathrm{div}_{\mathbf{X}}(J\mathbf{J}^{-1}{}^n\hat{\mathbf{u}})\cdot\hat{\mathbf{D}}\left({}^n\hat{\mathbf{u}},\frac{\partial\mathbf{J}}{\partial\boldsymbol{\Phi}_{\mathrm{s}}}\right)\\
&+\mathrm{div}_{\mathbf{X}}\left(\frac{\partial J}{\partial\boldsymbol{\Phi}_{\mathrm{s}}}\mathbf{J}^{-1}{}^n\hat{\mathbf{u}}\right)\cdot\hat{\mathbf{D}}({}^n\hat{\mathbf{u}},\mathbf{J})+\mathrm{div}_{\mathbf{X}}\left(J\frac{\partial\mathbf{J}^{-1}}{\partial\boldsymbol{\Phi}_{\mathrm{s}}}{}^n\hat{\mathbf{u}}\right)\cdot\hat{\mathbf{D}}({}^n\hat{\mathbf{u}},\mathbf{J})\Bigg]\mathrm{d}v_{\mathbf{X}}\\
&-\int_B\bar{T}\Bigg[\hat{\mathbf{D}}\left({}^n\hat{\mathbf{u}},\frac{\partial\mathbf{J}}{\partial\boldsymbol{\Phi}_{\mathrm{s}}}\right)\cdot 2\mu\hat{\mathbf{D}}({}^n\hat{\mathbf{u}},\mathbf{J})+\hat{\mathbf{D}}({}^n\hat{\mathbf{u}},\mathbf{J})\cdot 2\mu\hat{\mathbf{D}}\left({}^n\hat{\mathbf{u}},\frac{\partial\mathbf{J}}{\partial\boldsymbol{\Phi}_{\mathrm{s}}}\right)\Bigg]J\mathrm{d}v_{\mathbf{X}}\\
&+\int_B\left[\hat{\mathbf{g}}\left(\bar{T},\frac{\partial\mathbf{J}}{\partial\boldsymbol{\Phi}_{\mathrm{s}}}\right)\cdot\hat{\mathbf{k}}\hat{\mathbf{g}}({}^n\hat{T},\mathbf{J})+\hat{\mathbf{g}}(\bar{T},\mathbf{J})\cdot\hat{\mathbf{k}}\hat{\mathbf{g}}\left({}^n\hat{T},\frac{\partial\mathbf{J}}{\partial\boldsymbol{\Phi}_{\mathrm{s}}}\right)\right]J\mathrm{d}v_{\mathbf{X}}.\end{aligned}\tag{39}$$

In addition, the rightmost integrals in equations (42) and (55) are eliminated.

After the primal analysis and pseudoanalysis have been performed, the pressure may be recovered from

$$p = \hat{p}J = -\frac{1}{\epsilon}\mathrm{div}_{\mathbf{X}}(J\mathbf{J}^{-1}\hat{\mathbf{u}}) \tag{40}$$

and its sensitivity $\partial p/\partial\Phi_i$ may be computed from an application of the product rule to equation (40):

$$\frac{\partial\hat{p}}{\partial\Phi_i} = -\frac{1}{\epsilon}\left[\mathrm{div}_{\mathbf{X}}\left(\frac{\partial J}{\partial\Phi_i}\mathbf{J}^{-1}\hat{\mathbf{u}} + J\frac{\partial\mathbf{J}^{-1}}{\partial\Phi_i}\hat{\mathbf{u}} + J\mathbf{J}^{-1}\frac{\partial\hat{\mathbf{u}}}{\partial\Phi_i}\right)\Big/ J - \mathrm{div}_{\mathbf{X}}(J\mathbf{J}^{-1}\hat{\mathbf{u}})\frac{\partial J}{\partial\Phi_i}\Big/ J^2\right]. \tag{41}$$

The evaluation of G and its sensitivity remains unchanged; see equations (22) and (45)–(51).

APPENDIX II: DETAILED DERIVATIVES

This appendix provides detailed expressions of the derivatives that appear in the tangent operator, the pseudoload vector and the response functional sensitivity.

The following derivatives are used to evaluate the tangent operator in equation (22):

$$\begin{aligned}\frac{\partial({}^nR)}{\partial({}^n\hat{\mathbf{u}})}\mathrm{d}\hat{\mathbf{u}} = \int_B \bar{\mathbf{u}}\cdot\hat{\rho}\left(\frac{\mathrm{d}\hat{\mathbf{u}}}{\Delta t} + \nabla_{\mathbf{X}}{}^n\hat{\mathbf{u}}\mathbf{J}^{-1}\mathrm{d}\hat{\mathbf{u}} + \nabla_{\mathbf{X}}\mathrm{d}\hat{\mathbf{u}}\mathbf{J}^{-1}{}^n\hat{\mathbf{u}}\right)J\mathrm{d}v_{\mathbf{X}}\\ + \int_B [\hat{\mathbf{D}}(\bar{\mathbf{u}},\mathbf{J})\cdot 2\hat{\mu}\hat{\mathbf{D}}(\mathrm{d}\hat{\mathbf{u}},\mathbf{J})]J\mathrm{d}v_{\mathbf{X}}\\ + \int_B \bar{T}[\hat{\rho}\mathrm{d}\hat{\mathbf{u}}\cdot\mathbf{J}^{-\mathrm{T}}\nabla_{\mathbf{X}}{}^n\hat{e} + \hat{\mathbf{D}}(\mathrm{d}\hat{\mathbf{u}},\mathbf{J})\cdot{}^n\hat{p}\mathbf{I}\\ - \hat{\mathbf{D}}({}^n\hat{\mathbf{u}},\mathbf{J})\cdot 4\hat{\mu}\hat{\mathbf{D}}(\mathrm{d}\hat{\mathbf{u}},\mathbf{J})]J\mathrm{d}v_{\mathbf{X}} + \int_B \bar{p}\mathbf{I}\cdot\hat{\mathbf{D}}(\mathrm{d}\hat{\mathbf{u}},\mathbf{J})J\mathrm{d}v_{\mathbf{X}},\end{aligned} \tag{42}$$

$$\begin{aligned}\frac{\partial({}^nR)}{\partial({}^n\hat{T})}\mathrm{d}\hat{T} = \int_B -\bar{\mathbf{u}}\cdot\hat{\rho}\frac{\partial({}^n\hat{\mathbf{b}})}{\partial({}^n\hat{T})}\mathrm{d}\hat{T}J\mathrm{d}v_{\mathbf{X}}\\ + \int_B \left(\hat{\mathbf{D}}(\bar{\mathbf{u}},\mathbf{J})\cdot 2\frac{\partial\hat{\mu}}{\partial({}^n\hat{T})}\mathrm{d}\hat{T}\hat{\mathbf{D}}({}^n\hat{\mathbf{u}},\mathbf{J})\right)J\mathrm{d}v_{\mathbf{X}}\\ + \int_B \bar{T}\hat{\rho}\left[\frac{[\partial({}^n\hat{e})/\partial({}^n\hat{T})]\mathrm{d}\hat{T}}{\Delta t} + {}^n\hat{\mathbf{u}}\cdot\mathbf{J}^{-\mathrm{T}}\nabla_{\mathbf{x}}\left(\frac{\partial({}^n\hat{e})}{\partial({}^n\hat{T})}\mathrm{d}\hat{T}\right) - \frac{\partial({}^n\hat{Q})}{\partial({}^n\hat{T})}\mathrm{d}\hat{T}\right]J\mathrm{d}v_{\mathbf{X}}\\ - \int_B \bar{T}\left(\hat{\mathbf{D}}({}^n\hat{\mathbf{u}},\mathbf{J})\cdot 2\frac{\partial\hat{\mu}}{\partial({}^n\hat{T})}\mathrm{d}\hat{T}\hat{\mathbf{D}}({}^n\hat{\mathbf{u}},\mathbf{J})\right)J\mathrm{d}v_{\mathbf{X}}\\ + \int_B \left(\hat{\mathbf{g}}(\bar{T},\mathbf{J})\frac{\partial\hat{\mathbf{k}}}{\partial({}^n\hat{T})}\mathrm{d}\hat{T}\hat{\mathbf{g}}({}^n\hat{T},\mathbf{J}) + \hat{\mathbf{g}}(\hat{T},\mathbf{J})\cdot\hat{\mathbf{k}}\hat{\mathbf{g}}(\mathrm{d}\hat{T},\mathbf{J})\right)J\mathrm{d}v_{\mathbf{X}}\\ + \int_{A_q} \bar{T}\frac{\partial({}^n\hat{q}^p)}{\partial({}^n\hat{T})}\mathrm{d}\hat{T}K\mathrm{d}a_{\mathbf{X}},\end{aligned} \tag{43}$$

$$\frac{\partial({}^nR)}{\partial({}^n\hat{p})}\mathrm{d}\hat{p} = \int_B [-\mathrm{d}\hat{p}\mathbf{I}\cdot\hat{\mathbf{D}}(\bar{\mathbf{u}},\mathbf{J}) + \bar{T}\mathrm{d}\hat{p}\mathbf{I}\cdot\hat{\mathbf{D}}({}^n\hat{\mathbf{u}},\mathbf{J})]J\mathrm{d}v_{\mathbf{X}}, \tag{44}$$

The derivatives of the response function (see equation (22)), $\partial G/\partial \mathbf{\Phi}$ and $\partial G/\partial({}^{M}\mathbf{U})$, which are required to evaluate the sensitivities (see equation (13)) in Section 3.2 are evaluated in partitioned form as

$$\frac{\partial G}{\partial \mathbf{\Phi}_{\mathrm{s}}} = \int_B \left(\frac{\partial \hat{f}}{\partial({}^{M}\hat{\boldsymbol{\tau}})} \frac{\partial({}^{M}\hat{\boldsymbol{\tau}})}{\partial \mathbf{\Phi}_{\mathrm{s}}} + \frac{\partial \hat{f}}{\partial({}^{M}\hat{\mathbf{D}})} \frac{\partial({}^{M}\hat{\mathbf{D}})}{\partial \Phi_{\mathrm{s}}} + \frac{\partial \hat{f}}{\partial({}^{M}\hat{\mathbf{q}})} \frac{\partial({}^{M}\hat{\mathbf{q}})}{\partial \mathbf{\Phi}_{\mathrm{s}}} + \frac{\partial \hat{f}}{\partial({}^{M}\hat{\mathbf{g}})} \frac{\partial({}^{M}\hat{\mathbf{g}})}{\partial \mathbf{\Phi}_{\mathrm{s}}} + \frac{\partial \hat{f}}{\partial \mathbf{\Phi}_{\mathrm{s}}} \right) J \mathrm{d}v_{\mathbf{X}} + \int_B \hat{f} \frac{\partial J}{\partial \mathbf{\Phi}_{\mathrm{s}}} \mathrm{d}v_{\mathbf{X}} + \int_A \left(\frac{\partial \hat{h}}{\partial \mathbf{\Phi}_{\mathrm{s}}} K + \hat{h} \frac{\partial K}{\partial \mathbf{\Phi}_{\mathrm{s}}} \right) \mathrm{d}a_{\mathbf{X}} + \int_{A_t} \frac{\partial \hat{h}}{\partial({}^{M}\hat{\mathbf{t}})} \frac{\partial({}^{M}\hat{\mathbf{t}})}{\partial \mathbf{\Phi}_{\mathrm{s}}} K \mathrm{d}a_{\mathbf{X}}, \tag{45}$$

$$\frac{\partial G}{\partial \mathbf{\Phi}_{\mathrm{m}}} = \int_B \left(\frac{\partial \hat{f}}{\partial({}^{M}\hat{\boldsymbol{\tau}})} \frac{\partial({}^{M}\hat{\boldsymbol{\tau}})}{\partial \mathbf{\Phi}_{\mathrm{m}}} + \frac{\partial \hat{f}}{\partial({}^{M}\hat{e})} \frac{\partial({}^{M}\hat{e})}{\partial \mathbf{\Phi}_{\mathrm{m}}} + \frac{\partial \hat{f}}{\partial({}^{M}\hat{\mathbf{q}})} \frac{\partial({}^{M}\hat{\mathbf{q}})}{\partial \mathbf{\Phi}_{m}} + \frac{\partial \hat{f}}{\partial \mathbf{\Phi}_{\mathrm{m}}} \right) J \mathrm{d}v_{\mathbf{X}} + \int_A \frac{\partial \hat{h}}{\partial \mathbf{\Phi}_{\mathrm{m}}} K \mathrm{d}a_{\mathbf{X}} + \int_{A_t} \frac{\partial \hat{h}}{\partial({}^{M}\hat{\mathbf{t}})} \frac{\partial({}^{M}\hat{\mathbf{t}})}{\partial \mathbf{\Phi}_{\mathrm{m}}} K \mathrm{d}a_{\mathbf{X}} + \int_{A_q} \frac{\partial \hat{h}}{\partial({}^{M}\hat{q}^{\mathrm{s}})} \frac{\partial({}^{M}\hat{q}^{\mathrm{s}})}{\partial \mathbf{\Phi}^{\mathrm{m}}} K \mathrm{d}a_{\mathbf{X}}, \tag{46}$$

$$\frac{\partial G}{\partial \mathbf{\Phi}_{\mathrm{ld}}} = \int_B \frac{\partial \hat{f}}{\partial \mathbf{\Phi}_{\mathrm{ld}}} J \mathrm{d}v_{\mathbf{X}} + \int_A \frac{\partial \hat{h}}{\partial \mathbf{\Phi}_{\mathrm{ld}}} K \mathrm{d}a_{\mathbf{X}} + \int_{A_t} \frac{\partial \hat{h}}{\partial({}^{M}\hat{t})} \frac{\partial({}^{M}\hat{\mathbf{t}})}{\partial \mathbf{\Phi}_{\mathrm{ld}}} K \mathrm{d}a_{\mathbf{X}} + \int_{A_q} \frac{\partial \hat{h}}{\partial({}^{M}\hat{q}^{s})} \frac{\partial({}^{M}\hat{q}^{\mathrm{s}})}{\partial \mathbf{\Phi}_{\mathrm{ld}}} K \mathrm{d}a_{\mathbf{X}} + \int_{A_u} \frac{\partial \hat{h}}{\partial({}^{M}\hat{\mathbf{u}})} \frac{\partial({}^{M}\hat{\mathbf{u}})}{\partial \mathbf{\Phi}_{\mathrm{ld}}} K_{\mathrm{d}} a_{\mathbf{X}} + \int_{A_T} \frac{\partial \hat{h}}{\partial({}^{M}\hat{T})} \frac{\partial({}^{M}\hat{T})}{\partial \mathbf{\Phi}_{\mathrm{ld}}} K \mathrm{d}a^{\mathbf{X}}, \tag{47}$$

$$\frac{\partial G}{\partial({}^{M}\hat{\mathbf{u}})} = \int_B \left(\frac{\partial \hat{f}}{\partial({}^{M}\hat{\mathbf{u}})} + \frac{\partial \hat{f}}{\partial({}^{M}\hat{\boldsymbol{\tau}})} \frac{\partial({}^{M}\hat{\boldsymbol{\tau}})}{\partial({}^{M}\hat{\mathbf{u}})} + \frac{\partial \hat{f}}{\partial({}^{M}\hat{\mathbf{D}})} \frac{\partial({}^{M}\hat{\mathbf{D}})}{\partial({}^{M}\hat{\mathbf{u}})} \right) J \mathrm{d}v_{\mathbf{X}} + \int_{A_t} \frac{\partial \hat{h}}{\partial({}^{M}\hat{\mathbf{u}})} K \mathrm{d}a_{\mathbf{X}} + \int_{A_u} \frac{\partial \hat{h}}{\partial({}^{M}\hat{\mathbf{t}})} \frac{\partial({}^{M}\hat{\mathbf{t}})}{\partial {}^{M}\hat{\mathbf{u}}} K \mathrm{d}a_{\mathbf{X}}, \tag{48}$$

$$\frac{\partial G}{\partial({}^{M}\hat{T})} = \int_B \left(\frac{\partial \hat{f}}{\partial({}^{M}\hat{\boldsymbol{\tau}})} \frac{\partial({}^{M}\hat{\boldsymbol{\tau}})}{\partial({}^{M}\hat{T})} + \frac{\partial \hat{f}}{\partial({}^{M}\hat{T})} + \frac{\partial \hat{f}}{\partial({}^{M}\hat{e})} \frac{\partial({}^{M}\hat{e})}{\partial({}^{M}\hat{T})} + \frac{\partial \hat{f}}{\partial({}^{M}\hat{\mathbf{q}})} \frac{\partial({}^{M}\hat{\mathbf{q}})}{\partial({}^{M}\hat{T})} + \frac{\partial \hat{f}}{\partial({}^{M}\hat{\mathbf{g}})} \frac{\partial({}^{M}\hat{\mathbf{g}})}{\partial({}^{M}\hat{T})} \right) J \mathrm{d}v_{\mathbf{X}} + \int_{A_q} \frac{\partial \hat{h}}{\partial({}^{M}\hat{T})} K \mathrm{d}a_{\mathbf{X}} + \int_{A_T} \frac{\partial \hat{h}}{\partial({}^{M}\hat{q}^{\mathrm{s}})} \frac{\partial({}^{M}\hat{q}^{\mathrm{s}})}{\partial({}^{M}\hat{T})} K \mathrm{d}a_{\mathbf{X}}, \tag{49}$$

$$\frac{\partial G}{\partial({}^{M}\hat{p})} = \int_B \left(\frac{\partial \hat{f}}{\partial({}^{M}\hat{p})} + \frac{\partial \hat{f}}{\partial({}^{M}\hat{\boldsymbol{\tau}})} \frac{\partial({}^{M}\hat{\boldsymbol{\tau}})}{\partial({}^{M}\hat{p})} \right) J \mathrm{d}v_{\mathbf{X}} + \int_A \frac{\partial \hat{h}}{\partial({}^{M}\hat{p})} K \mathrm{d}a_{\mathbf{X}} + \int_{A_u} \frac{\partial \hat{h}}{\partial({}^{M}\hat{\mathbf{t}})} \frac{\partial({}^{M}\hat{\mathbf{t}})}{\partial({}^{M}\hat{p})} K \mathrm{d}a_{\mathbf{X}}, \tag{50}$$

where, from equations (16) and (20) and letting M equal n, we have

$$\frac{\partial({}^n\hat{\boldsymbol{\tau}})}{\partial \boldsymbol{\Phi}_s} = 2\mu \frac{\partial({}^n\hat{\mathbf{D}})}{\partial \boldsymbol{\Phi}_s},$$

$$\frac{\partial({}^n\hat{\boldsymbol{\tau}})}{\partial \boldsymbol{\Phi}_m} = 2\frac{\partial \mu}{\partial \boldsymbol{\Phi}_m}\,{}^n\hat{\mathbf{D}},$$

$$\frac{\partial({}^n\hat{\boldsymbol{\tau}})}{\partial({}^n\hat{\mathbf{u}})} = 2\mu \frac{\partial({}^n\hat{\mathbf{D}})}{\partial({}^n\hat{\mathbf{u}})},$$

$$\frac{\partial({}^n\hat{\boldsymbol{\tau}})}{\partial({}^n\hat{T})} = 2\frac{\partial \mu}{\partial({}^n\hat{T})}\,{}^n\hat{\mathbf{D}},$$

$$\frac{\partial({}^n\hat{\tau})}{\partial({}^n\hat{p})} = -\mathbf{I},$$

$$\frac{\partial({}^n\hat{\mathbf{D}})}{\partial \boldsymbol{\Phi}_s} = {}^n\hat{\mathbf{D}}\left({}^n\hat{\mathbf{u}}, \frac{\partial \mathbf{J}}{\partial \boldsymbol{\Phi}_s}\right),$$

$$\frac{\partial({}^n\hat{\mathbf{q}})}{\partial \boldsymbol{\Phi}_s} = -\hat{\mathbf{k}}\frac{\partial({}^n\hat{\mathbf{g}})}{\partial \boldsymbol{\Phi}_s},$$

$$\frac{\partial({}^n\hat{\mathbf{q}})}{\partial \boldsymbol{\Phi}_m} = -\frac{\partial \hat{\mathbf{k}}}{\partial \boldsymbol{\Phi}_m}\,{}^n\hat{\mathbf{g}},$$

$$\frac{\partial({}^n\hat{\mathbf{q}})}{\partial T} = -\frac{\partial \hat{\mathbf{k}}}{\partial \hat{T}}\,{}^n\hat{\mathbf{g}} - \hat{\mathbf{k}}\frac{\partial({}^n\hat{\mathbf{g}})}{\partial \hat{T}},$$

$$\frac{\partial({}^n\hat{\mathbf{g}})}{\partial \boldsymbol{\Phi}_s} = {}^n\hat{\mathbf{g}}\left({}^n\hat{T}, \frac{\partial \mathbf{J}}{\partial \boldsymbol{\Phi}_s}\right). \tag{51}$$

The derivatives as of yet undefined in equation (24) are as follows:

$$\frac{\partial({}^nR)}{\partial({}^{n-1}\hat{\mathbf{u}})} = \int_B -\frac{\bar{\mathbf{u}}\hat{\rho}}{\Delta t} J \mathrm{d}v_{\mathbf{X}}, \tag{52}$$

$$\frac{\partial({}^nR)}{\partial({}^{n-1}\hat{T})} = \int_B -\frac{\bar{T}\hat{\rho}\,\partial({}^{n-1}\hat{e})/\partial({}^{n-1}\hat{T})}{\Delta t} J \mathrm{d}v^{\mathbf{X}}, \tag{53}$$

$$\frac{\partial({}^nR)}{\partial({}^{n-1}\hat{p})} = 0, \tag{54}$$

$$\frac{\partial({}^{n}R)}{\partial \boldsymbol{\Phi}_s} = \int_B \left[\bar{\mathbf{u}} \cdot \hat{\rho} \left(\frac{{}^{n}\hat{\mathbf{u}} - {}^{n-1}\hat{\mathbf{u}}}{\Delta t} + \nabla_{\mathbf{X}} {}^{n}\hat{\mathbf{u}} \mathbf{J}^{-1} {}^{n}\hat{\mathbf{u}} - {}^{n}\hat{\mathbf{b}} \right) \right.$$

$$\left. - {}^{n}\hat{p}\mathbf{I} \cdot \hat{\mathbf{D}}(\bar{\mathbf{u}}, \mathbf{J}) + \hat{\mathbf{D}}(\bar{\mathbf{u}}, \mathbf{J}) \cdot 2\hat{\mu}\hat{\mathbf{D}}({}^{n}\hat{\mathbf{u}}, \mathbf{J}) \right) \Bigg] \frac{\partial J}{\partial \boldsymbol{\Phi}_s} \mathrm{d}v_{\mathbf{X}}$$

$$- \int_{A_t} \bar{\mathbf{u}} \cdot \hat{\mathbf{t}}^{\mathrm{p}} \frac{\partial K}{\partial \boldsymbol{\Phi}_s} \mathrm{d}a_{\mathbf{X}} + \int_B \bar{\mathbf{u}} \cdot \hat{\rho} \left(\nabla_{\mathbf{X}} {}^{n}\hat{\mathbf{u}} \frac{\partial \mathbf{J}^{-1}}{\partial \boldsymbol{\Phi}_s} {}^{n}\hat{\mathbf{u}} \right) J \mathrm{d}v_{\mathbf{X}}$$

$$+ \int_B \left[\hat{\mathbf{D}} \left(\bar{\mathbf{u}}, \frac{\partial \mathbf{J}}{\partial \boldsymbol{\Phi}_s} \right) \cdot 2\hat{\mu}\hat{\mathbf{D}}({}^{n}\hat{\mathbf{u}}, \mathbf{J}) + \hat{\mathbf{D}}(\bar{\mathbf{u}}, \mathbf{J}) \cdot 2\hat{\mu}\hat{\mathbf{D}} \left({}^{n}\hat{\mathbf{u}}, \frac{\partial \mathbf{J}}{\partial \boldsymbol{\Phi}_s} \right) \right] J \mathrm{d}v_{\mathbf{X}}$$

$$- \int_B {}^{n}\hat{p}\mathbf{I} \cdot \hat{\mathbf{D}} \left(\bar{\mathbf{u}}, \frac{\partial \mathbf{J}}{\partial \boldsymbol{\Phi}_s} \right) J \mathrm{d}v^{\mathbf{X}}$$

$$+ \int_B \bar{T}\hat{\rho} \left(\frac{{}^{n}\hat{e} - {}^{n-1}\hat{e}}{\Delta t} + {}^{n}\hat{\mathbf{u}} \cdot J^{-\mathrm{T}} \nabla_{\mathbf{X}} {}^{n}\hat{e} - {}^{n}\hat{Q} \right) \frac{\partial J}{\partial \boldsymbol{\Phi}_s} \mathrm{d}v^{\mathbf{X}}$$

$$+ \int_B [\hat{\mathbf{g}}(\bar{T}, \mathbf{J}) \cdot \hat{\mathbf{k}}\hat{\mathbf{g}}({}^{n}\hat{T}, \mathbf{J}) + \bar{T}{}^{n}\hat{p}\mathbf{I} \cdot \hat{\mathbf{D}}({}^{n}\hat{\mathbf{u}}, \mathbf{J})] \frac{\partial J}{\partial \boldsymbol{\Phi}_s} \mathrm{d}v^{\mathbf{X}}$$

$$+ \int_{A_q} \bar{T}\hat{q}^{\mathrm{p}} \frac{\partial K}{\partial \boldsymbol{\Phi}_s} \mathrm{d}a_{\mathbf{X}} - \int_B \hat{T} \left(\hat{\mathbf{D}}({}^{n}\hat{\mathbf{u}}, \mathbf{J}) \cdot 2\mu\hat{\mathbf{D}}({}^{n}\hat{\mathbf{u}}, \mathbf{J}) \frac{\partial J}{\partial \boldsymbol{\Phi}_s} \right) \mathrm{d}v_{\mathbf{X}}$$

$$+ \int_{\mathrm{B}} \bar{T}\hat{\rho} \left({}^{n}\hat{\mathbf{u}} \cdot \frac{\partial \mathbf{J}^{-\mathrm{T}}}{\partial \boldsymbol{\Phi}_s} \nabla_{\mathbf{X}} {}^{n}\hat{e} \right) J \mathrm{d}v_{\mathbf{X}} + \int_B \bar{T}{}^{n}\hat{p}\mathbf{I} \cdot \hat{\mathbf{D}} \left({}^{n}\hat{\mathbf{u}}, \frac{\partial \mathbf{J}}{\partial \boldsymbol{\Phi}_s} \right) J \mathrm{d}v_{\mathbf{X}}$$

$$- \int_B \bar{T} \left[\hat{\mathbf{D}} \left({}^{n}\hat{\mathbf{u}}, \frac{\partial \mathbf{J}}{\partial \boldsymbol{\Phi}_s} \right) \cdot 2\mu\hat{\mathbf{D}}({}^{n}\hat{\mathbf{u}}, \mathbf{J}) + \hat{\mathbf{D}}({}^{n}\hat{\mathbf{u}}, \mathbf{J}) \cdot 2\mu\hat{\mathbf{D}} \left({}^{n}\hat{\mathbf{u}}, \frac{\partial \mathbf{J}}{\partial \boldsymbol{\Phi}_s} \right) \right] J \mathrm{d}v_{\mathbf{X}}$$

$$+ \int_B \left[\hat{\mathbf{g}} \left(\bar{T}, \frac{\partial \mathbf{J}}{\partial \boldsymbol{\Phi}_s} \right) \cdot \hat{\mathbf{k}}\hat{\mathbf{g}}({}^{n}\hat{T}, \mathbf{J}) + \hat{\mathbf{g}}(\bar{T}, \mathbf{J}) \cdot \hat{\mathbf{k}}\hat{\mathbf{g}} \left({}^{n}\hat{T}, \frac{\partial \mathbf{J}}{\partial \boldsymbol{\Phi}_s} \right) \right] J \mathrm{d}v_{\mathbf{X}}$$

$$+ \int_B \left[\bar{p}\mathbf{I} \cdot \hat{\mathbf{D}} \left({}^{n}\hat{\mathbf{u}}, \frac{\partial \mathbf{J}}{\partial \boldsymbol{\Phi}_s} \right) J + \bar{p}\mathbf{I} \cdot \hat{\mathbf{D}}({}^{n}\hat{\mathbf{u}}, \mathbf{J}) \frac{\partial J}{\partial \boldsymbol{\Phi}_s} \right] \mathrm{d}v_{\mathbf{X}}, \tag{55}$$

$$\frac{\partial({}^nR)}{\partial \boldsymbol{\Phi}_m} = \int_B \Bigg[\bar{\mathbf{u}} \cdot \frac{\partial \hat{\rho}}{\partial \boldsymbol{\Phi}_m} \left(\frac{{}^n\hat{\mathbf{u}} - {}^{n-1}\hat{\mathbf{u}}}{\Delta t} + \nabla_{\mathbf{X}} {}^n\hat{\mathbf{u}} \mathbf{J}^{-1} {}^n\hat{\mathbf{u}} - {}^n\hat{\mathbf{b}} \right)$$
$$+ \hat{\mathbf{D}}(\bar{\mathbf{u}}, \mathbf{J}) \cdot 2 \frac{\partial \hat{\mu}}{\partial \boldsymbol{\Phi}_m} \hat{\mathbf{D}}({}^n\hat{\mathbf{u}}, \mathbf{J}) \Bigg] J \mathrm{d}v_{\mathbf{X}}$$
$$+ \int_B \bar{T} \frac{\partial \hat{\rho}}{\partial \boldsymbol{\Phi}_m} \left(\frac{{}^n\hat{e} - {}^{n-1}\hat{e}}{\Delta t} + {}^n\hat{\mathbf{u}} \cdot \mathbf{J}^{-\mathrm{T}} \nabla_{\mathbf{X}} {}^n\hat{e} - \hat{Q} \right) J \mathrm{d}v_{\mathbf{X}}$$
$$+ \int_B \bar{T} \hat{\rho} \left[\frac{\partial({}^n\hat{e})/\partial \boldsymbol{\Phi}_m - \partial({}^{n-1}\hat{e})/\partial \boldsymbol{\Phi}_m}{\Delta t} + {}^n\hat{\mathbf{u}} \cdot \mathbf{J}^{-\mathrm{T}} \nabla_{\mathbf{X}} \left(\frac{\partial({}^n\hat{e})}{\partial \boldsymbol{\Phi}_m} \right) \right] J \mathrm{d}v_{\mathbf{X}}$$
$$- \int_B \bar{T} \left(\hat{\mathbf{D}}({}^n\hat{\mathbf{u}}, \mathbf{J}) \cdot 2 \frac{\partial \mu}{\partial \boldsymbol{\Phi}_m} \hat{\mathbf{D}}({}^n\hat{\mathbf{u}}, \mathbf{J}) \right) J \mathrm{d}v_{\mathbf{X}}$$
$$+ \int_B \hat{\mathbf{g}}(\bar{T}, \mathbf{J}) \cdot \frac{\partial \hat{\mathbf{k}}}{\partial \boldsymbol{\Phi}_m} \hat{\mathbf{g}}({}^n\hat{T}, \mathbf{J}) J \mathrm{d}v_{\mathbf{X}}$$
$$+ \int_{A_q} \bar{T} \frac{\partial({}^n\hat{q}^p)}{\partial \boldsymbol{\Phi}_m} K \mathrm{d}a_{\mathbf{X}}, \tag{56}$$

$$\frac{\partial({}^nR)}{\partial \boldsymbol{\Phi}_{ld}} = -\int_B \bar{\mathbf{u}} \cdot \rho \frac{\partial({}^n\hat{\mathbf{b}})}{\partial \boldsymbol{\Phi}_{ld}} J \mathrm{d}v_{\mathbf{X}} - \int_{A_t} \bar{\mathbf{u}} \cdot \frac{\partial({}^n\hat{\mathbf{t}}^p)}{\partial \boldsymbol{\Phi}_{ld}} K \mathrm{d}a_{\mathbf{X}} - \int_B \bar{T} \rho \frac{\partial({}^n\hat{Q})}{\partial \boldsymbol{\Phi}_{ld}} J \mathrm{d}v_{\mathbf{X}} + \int_{A_q} \bar{T} \frac{\partial({}^n\hat{q}^p)}{\partial \boldsymbol{\Phi}_{ld}} K \mathrm{d}a_{\mathbf{X}}. \tag{57}$$

The derivatives for the tangent operator of equation (31) are

$$\frac{\partial R}{\partial \hat{\mathbf{u}}} \mathrm{d}\hat{\mathbf{u}} = \int_B \bar{\mathbf{u}} \cdot \hat{\rho} (\nabla_{\mathbf{X}} \hat{\mathbf{u}} \mathbf{J}^{-1} \mathrm{d}\hat{\mathbf{u}} + \nabla_{\mathbf{X}} \mathrm{d}\hat{\mathbf{u}} \mathbf{J}^{-1} \hat{\mathbf{u}}) J \mathrm{d}v_{\mathbf{X}} + \int_B \left(\hat{\mathbf{D}}(\bar{\mathbf{u}}, \mathbf{J}) \cdot 2 \frac{\partial \hat{\mu}_t(\hat{l}_m, \hat{\mathbf{D}})}{\partial(\hat{\mathbf{u}})} \mathrm{d}\hat{\mathbf{u}} \hat{\mathbf{D}}(\hat{\mathbf{u}}, \mathbf{J}) \right) J \mathrm{d}v_{\mathbf{X}}$$
$$+ \int_B \{ \hat{\mathbf{D}}(\bar{\mathbf{u}}, \mathbf{J}) \cdot 2[\hat{\mu} + \hat{\mu}_t(\hat{l}_m, \hat{\mathbf{D}})] \hat{\mathbf{D}}(\mathrm{d}\hat{\mathbf{u}}, \mathbf{J}) \} J \mathrm{d}v_{\mathbf{X}} + \int_B \hat{p} \mathbf{I} \cdot \hat{\mathbf{D}}(\mathrm{d}\hat{\mathbf{u}}, \mathbf{J}) \mathrm{d}v_{\mathbf{X}}, \tag{58}$$

$$\frac{\partial R}{\partial \hat{p}} \mathrm{d}\hat{p} = \int_B [-\mathrm{d}\hat{p} \mathbf{I} \cdot \hat{\mathbf{D}}(\bar{\mathbf{u}}, \mathbf{J})] J \mathrm{d}v_{\mathbf{X}}, \tag{59}$$

$$\frac{\partial \hat{\mu}_t(\hat{l}_m, \hat{\mathbf{D}})}{\partial(\hat{\mathbf{u}})} \mathrm{d}\hat{\mathbf{u}} = \rho \hat{l}_m^2 \left(2 \frac{\hat{\mathbf{D}}(\mathrm{d}\hat{\mathbf{u}}, \mathbf{J}) \cdot \hat{\mathbf{D}}(\hat{\mathbf{u}}, \mathbf{J})}{[\hat{\mathbf{D}}(\hat{\mathbf{u}}, \mathbf{J}) \cdot \hat{\mathbf{D}}(\hat{\mathbf{u}}, \mathbf{J})]^{1/2}} \right). \tag{60}$$

The derivative expressions in

$$\left[\frac{\partial({}^nR)}{\partial \boldsymbol{\Phi}_s} \quad \frac{\partial({}^nR)}{\partial \boldsymbol{\Phi}_m} \quad \frac{\partial({}^nR)}{\partial \boldsymbol{\Phi}_{ld}} \right]$$

(see equation (24)) for the turbulent flow residual equation (28) are

$$\begin{aligned}\frac{\partial R}{\partial \boldsymbol{\Phi}_s} = \int_B & \bar{\mathbf{u}} \cdot \hat{\rho}(\nabla_{\mathbf{X}} \hat{\mathbf{u}} \mathbf{J}^{-1} \hat{\mathbf{u}} - \hat{\mathbf{b}}) \\ & - \hat{p}\mathbf{I} \cdot \hat{\mathbf{D}}(\bar{\mathbf{u}}, \mathbf{J}) + \hat{\mathbf{D}}(\bar{\mathbf{u}}, \mathbf{J}) \cdot 2[\hat{\mu} + \hat{\mu}_t(\hat{l}_m, \hat{\mathbf{D}})]\hat{\mathbf{D}}(\hat{\mathbf{u}}, \mathbf{J})\} \frac{\partial J}{\partial \boldsymbol{\Phi}_s} \mathrm{d}v_{\mathbf{X}} \\ & - \int_{A_t} \bar{\mathbf{u}} \cdot \bar{\mathbf{t}}^p \frac{\partial K}{\partial \boldsymbol{\Phi}_s} \mathrm{d}a_{\mathbf{X}} + \int_B \bar{\mathbf{u}} \cdot \hat{\rho} \left(\nabla_{\mathbf{X}} \hat{\mathbf{u}} \frac{\partial \mathbf{J}_{-1}}{\partial \boldsymbol{\Phi}_s} \hat{\mathbf{u}} \right) J \mathrm{d}v_{\mathbf{X}} \\ & - \int_B \hat{p}\mathbf{I} \cdot \hat{\mathbf{D}} \left(\bar{\mathbf{u}}, \frac{\partial \mathbf{J}}{\partial \boldsymbol{\Phi}_s} \right) J \mathrm{d}v_{\mathbf{X}} \\ & + \int_B \left[\hat{\mathbf{D}} \left(\bar{\mathbf{u}}, \frac{\partial \mathbf{J}}{\partial \boldsymbol{\Phi}_s} \right) \cdot 2[\hat{\mu}\hat{\mu}_t(\hat{l}_m, \hat{\mathbf{D}})]\hat{\mathbf{D}}(\hat{\mathbf{u}}, \mathbf{J}) \right. \\ & + \hat{\mathbf{D}}(\bar{\mathbf{u}}, \mathbf{J}) \cdot 2 \frac{\partial \hat{\mu}_t(\hat{l}_m, \hat{\mathbf{D}})}{\partial \boldsymbol{\Phi}_s} \hat{\mathbf{D}}(\hat{\mathbf{u}}, \mathbf{J}) \\ & \left. + \hat{\mathbf{D}}(\bar{\mathbf{u}}, \mathbf{J}) \cdot 2[\hat{\mu} + \hat{\mu}_t(\hat{l}_m, \hat{\mathbf{D}})]\hat{\mathbf{D}} \left(\hat{\mathbf{u}}, \frac{\partial \mathbf{J}}{\partial \boldsymbol{\Phi}_s} \right) \right] J \mathrm{d}_{\mathbf{X}} \\ & + \int_B \left[\bar{p}\mathbf{I} \cdot \hat{\mathbf{D}} \left(\hat{\mathbf{u}}, \frac{\partial \mathbf{J}}{\partial \boldsymbol{\Phi}_s} \right) J + \bar{p}\mathbf{I} \cdot \hat{\mathbf{D}}(\hat{\mathbf{u}}, \mathbf{J}) \frac{\partial J}{\partial \boldsymbol{\Phi}_s} \right] \mathrm{d}v_{\mathbf{X}}, \end{aligned} \tag{61}$$

$$\frac{\partial R}{\partial \boldsymbol{\Phi}_m} = \int_B \left(\bar{\mathbf{u}} \cdot \frac{\partial \hat{\rho}}{\partial \boldsymbol{\Phi}_m} \left(\nabla_{\mathbf{X}} \hat{\mathbf{u}} \mathbf{J}^{-1} \hat{\mathbf{u}} - \hat{\mathbf{b}} \right) + \hat{\mathbf{D}}(\bar{\mathbf{u}}, \mathbf{J}) \cdot 2 \frac{\partial \hat{\mu}}{\partial \boldsymbol{\Phi}_m} \hat{\mathbf{D}}(\hat{\mathbf{u}}, \mathbf{J}) \right) J \mathrm{d}v_{\mathbf{X}}, \tag{62}$$

$$\frac{\partial R}{\partial \boldsymbol{\Phi}_{ld}} = - \int_B \bar{\mathbf{u}} \cdot \rho \frac{\partial \hat{\mathbf{b}}}{\partial \boldsymbol{\Phi}_{ld}} J \mathrm{d}v_{\mathbf{X}} - \int_{A_t} \bar{\mathbf{u}} \cdot \frac{\partial \hat{\mathbf{t}}^p}{\partial \boldsymbol{\Phi}_{ld}} K \mathrm{d}a_{\mathbf{X}}, \tag{63}$$

where

$$\frac{\partial \hat{\mu}_t(\hat{l}_m, \hat{\mathbf{D}})}{\partial \boldsymbol{\Phi}_x} = 2\rho \hat{l}_m \frac{\partial \hat{l}_m}{\partial \boldsymbol{\Phi}_s} [2\hat{\mathbf{D}}(\hat{\mathbf{u}}, \mathbf{J}) \cdot \hat{\mathbf{D}}(\hat{\mathbf{u}}, \mathbf{J})]^{1/2} + 2\rho \hat{l}_m^2 \left(\frac{\hat{\mathbf{D}}(\hat{\mathbf{u}}, \partial \mathbf{J}/\partial \boldsymbol{\Phi}_s) \cdot \hat{\mathbf{D}}(\hat{\mathbf{u}}, \mathbf{J})}{[\hat{\mathbf{D}}(\hat{\mathbf{u}}, \mathbf{J}) \cdot \hat{\mathbf{D}}(\hat{\mathbf{u}}, \mathbf{J})]^{1/2}} \right). \tag{64}$$

REFERENCES

1. R. M. Hicks and P. A. Henne, 'Wing design by numerical optimization', *J. Aircraft*, **15**, 407–412 (1978).
2. K. K. Mani, 'Design using Euler equations', *AIAA Paper 84-2166*, 1984.
3. K. Lee and S. Eyi, 'Aerodynamic design via optimization', *J. Aircraft*, **29**, 1012–1029 (1992).
4. R. Glowinski, T. W. Pan, A. J. Kearsley and J. Periaux, 'Numerical simulation and optimal shape for viscous flow by a fictitious domain method', *Int. j. numer. methods fluids*, **20**, 695–711 (1995).
5. R. T. Haftka, 'Techniques for thermal sensitivity analysis', *Int. j. numer. methods eng.*, **17**, 71–80 (1981).
6. R. A. Meric, 'Boundary integral equation and conjugate gradient methods for optimal boundary heating of solids', *Int. J. Heat Mass Transfer*, **26**, 261–267 (1983).
7. R. A. Meric, 'Boundary element methods for optmization of distributed parameter systems', *Int. j. numer. methods in eng.*, **20**, 1291–1306 (1984).
8. R. A. Meric, 'Optimal loading of solids by the boundary element method', *Int. J. Eng. Sci.*, **23**, 1101–1111 (1985).
9. D. A. Tortorelli and R. B. Haber, 'First-order design sensitivities for transient conduction problems by an adjoint method', *Int. j. numer. methods eng.*, **28**, 733–752 (1989).
10. D. A. Tortorelli, R. B. Haber and S. C. -Y. Lu, 'Design sensitivity analysis for nonlinear thermal systems', *Comput. Methods Appl. Mech. Eng.*, **77**, 61–77 (1989).
11. K. Dems, 'Sensitivity analysis in thermal problems—I: Variation of material parameters with a fixed domain', *J. Thermal Stresses*, **9**, 303–324 (1986).
12. K. Dems, 'Sensitivity anlaysis in thermal problems—II: Structure shape variation', J. Thermal Stresses, **10**, 1–16 (1987).

13. D. A. Tortorelli, M. M. Tiller and J. A. Dantzig, 'Optimal design of nonlineaer parabolic systems. Part I: Fixed spatial domains with applications to process optimization', *Comput. Methods Appl. Mech. Eng.*, **113**, 141–155 (1994).
14. O. Baysal and M. E. Eleshaky, 'Aerodynamic sensitivity analysis methods for the compressible Euler equations', *J. Fluids Eng.*, **113**, 681–688 (1991).
15. O. Baysal and M. E. Eleshaky, 'Aerodynamic design optimization using sensitivity analysis and computational fluid dynamics', *AIAA J.*, **30**, 718–725 (1992).
16. M. E. Eleshaky and O.Baysal, 'Airfoil shape optimization using sensitivity analysis on viscous flow equations', *J. Fluids Eng.*, **115**, 75–84 (1993).
17. H. Cabuk, C.-H. Sung and V. Modi, 'Adjoint operator approach to shape design for internal incompressible flows', *Proc. Third Int. Conf. on Inverse Design Concepts and Optimization in Engineering Sciences*, Washington D.C., October 1991, Wert Boolebinding, Grantville, PA, 1991, pp. 391–404.
18. G. S. Dulikravich, 'Aerodynamic shape design and optimization', *AIAA Paper 91-0476*, 1991.
19. G. R. Shubin and P. D. Frank, 'A comparison of two closely-related approaches to aerodynamic design optimization', *Proc. Third Int. Conf. on Inverse Design Concepts and Optimization in Engineering Sciences*, Washington D.C., October 1991, Wert Boolebinding, Grantville, PA, 1991, pp. 67–78.
20. M. Behr, J. Liou, R. Shih and T. E. Tezduyar, 'Vorticity–streamfunction formulation of unsteady incompressible flow past a cylinder: sensitivity of the compared flow field to the location of the outflow boundary', *Int. j. numer. methods fluids*, **12**, 323–342 (1991).
21. R. M. Fearn, T. Mullin and K. A. Cliffe, 'Nonlinear flow phenomena in a symmetric sudden expansion', *J. Fluid Mech.*, **211**, 595–608 (1990).
22. B. E. Launder, A. P. Morse, W. Rodi and D. B. Spalding, 'The prediction of free-shear flows—a comparison of the performance of six turbulence models', *NASA SP 320*, 1973.
23. B. E. Launder and D. B. Spalding, 'The numerical computation of turbulent flows', *Comput. Methods Appl. Mech. Eng.*, **3**, 269–289 (1974).
24. W. Rodi, *Turbulence Models and Their Application in Hydraulics: A State of the Art Review*, University of Karlsruhe, Karlsruhe, 1980.
25. D. A. Tortorelli and Z. X. Wang, 'A systemaic approach to shape sensitivity analysis', *Int. J. Solids Struct.*, **30**, 1181–1212 (1993).
26. P. Michaleris, D. A. Tortorelli and C. A. Vidal, 'Tangent operators and sensitivity formulations for transient nonlinear coupled problems with applications to elasto-plasticity', *Int. j. numer. methods eng.*, **37**, 2471–2500 (1994).
27. C. G. Broyden, 'A class of methods for solving nonlinear simultaneous equations,' *Math. Comput.*, **19**, 577–593 (1965).
28. D. A. Tortorelli and P. Michaleris, 'Design sensitivity analysis: overview and review', *Inverse Prob. Eng.*, **1**, 71–105 (1994).
29. P. M. Gresho, R. L. Lee and R. L. Sani, 'On the time-dependent solution of the incompressible Navier–Stokes equations in two and three dimensions', in *Recent Advances in Numerical Methods in Fluids*, C. Taylor and K. Morgan (eds.), Pineridge, Swansea, 1980.
30. P. M. Gresho, S. T. Chan, R. L. Lee and C. D. Upson, 'A modified finite element method for solving the time-dependent, incompressible Navier–Stokes equations. Part I: Theory,' *Int. j. numer. methods fluids*, **4**, 557–598 (1984).
31. I. G. Currie, *Fundamental Mechanics of Fluids*, McGraw-Hill, New York, 1993.
32. C. Johnson, *Numerical Solution of Partial Differential Equations by the Finite Element Method*, Cambridge University Press, Cambridge, 1990.
33. P. Bradshaw, *An Introduction to Turbulence and Its Measurement*, Pergamon, Oxford, 1971.
34. H. Schlichting, *Boundary Layer Theory*, 6th edn, McGraw-Hill, New York, 1968.
35. Z. X. Wang, 'Computer-aided optimal design for laminar and turbulent fluid–thermal systems', *Ph.D. Thesis*, Department of Theoretical and Applied Mechanics, University of Illinois at Urbana-Champaign, Urbana, IL, 1995.
36. PDA Engineering, *Patran Plus User's Manual*, Vols I and II, Software Products Division, Costa Mesa, CA, 1990.
37. J. A. Tomasko, 'Parametric mapped mesh generators for shape sensitivity evaluation with application to casting optimization', *Master's Thesis*, Department of Mechanical and Industrial Engineering, University of Illinois at Urbana-Champaign, Urbana, IL, 1992.
38. D. A. Tortorelli, R. B. Haber and S. C. -Y. Lu, 'Adjoint sensitivity analysis for nonlinear dynamic thermoelastic systems', *AIAA J.*, **29**, 253–263 (1991).
39. M. S. Engelman, *FIDAP Theoretical Manual*, Fluid Dynamics International, Evanston, IL, 1993.
40. VMA Engineering, *DOT User's Manual, Version 3.0*, Vanderplaats, Miura, Miura & Associates, Goleta, CA, 1992.
41. R. Fletcher, 'A new approach to variable metric algorithms', *Comput. J.*, **13**, 317–322 (1970).
42. F. Durst and T. Loy, 'Investigations of laminar flow in a pipe with sudden contraction of cross sectional area', *Comput. Fluids*, **13**, 15–36 (1985).
43. W. I. Zangwill, *Nonlinear Programming; a Unified Approach*, Prentice-Hall, Englewood Cliffs, NJ, 1969.
44. G. N. Vanderplaats, Numerical Optimization Techniques for Engineering Design: With Applications, McGraw-Hill, New York, 1984.
45. C. Bischof, G. Whiffen, C. Shoemaker, A. Carle and A. Ross, 'Application of automatic differentiation to groundwater transport models', *Proc. Int. Conf. on Computational Methods in Water Resources*, Heidelberg, July 1994, A. Peters (ed.), Kluwer Academic Press, Dordrect, 1994, pp 173–182.
46. T. J. R. Hughes, *The Finite Element Method, Linear Static and Dynamic Finite Element Analysis*, Prentice-Hall, Englewood Cliffs, NJ, 1987.